CONTROLLED LATERAL AND PERPENDICULAR MOTION OF ATOMS ON METAL SURFACES

A THESIS
SUBMITTED TO THE DEPARTMENT OF PHYSICS
AND THE INSTITUTE OF ENGINEERING AND SCIENCE
OF BİLKENT UNIVERSITY
IN PARTIAL FULFILLMENT OF THE REQUIREMENTS
FOR THE DEGREE OF
MASTER OF SCIENCE

By
Alper Buldum
November 1994

CONTROLLED LATERAL AND PERPENDICULAR MOTION OF ATOMS ON METAL SURFACES

A THESIS

SUBMITTED TO THE DEPARTMENT OF PHYSICS

AND THE INSTITUTE OF ENGINEERING AND SCIENCE

OF BİLKENT UNIVERSITY

IN PARTIAL FULFILLMENT OF THE REQUIREMENTS

FOR THE DEGREE OF

MASTER OF SCIENCE

By

Alper Buldum

November 1994

I certify that I have read this thesis and that in my opinion it is fully adequate, in scope and in quality, as a dissertation for the degree of Master of Science.

Prof. Salim Çıracı (Supervisor)

I certify that I have read this thesis and that in my opinion it is fully adequate, in scope and in quality, as a dissertation for the degree of Master of Science.

Prof. Walter A. Harrison

I certify that I have read this thesis and that in my opinion it is fully adequate, in scope and in quality, as a dissertation for the degree of Master of Science.

Prof. Atilla Aydınlı

Approved for the Institute of Engineering and Science:

Prof. Mehmet Baray,
Director of Institute of Engineering and Science

Abstract

CONTROLLED LATERAL AND PERPENDICULAR MOTION OF ATOMS ON METAL SURFACES

Alper Buldum
M. S. in Physics
Supervisor: Prof. Salim Çıracı
November 1994

Nanoscale modification of matter has been the subject of interest. Recently, several experimental studies have demonstrated that by using a scanning tunneling microscope one can translate atoms on metal surfaces to a desired position. Furthermore, it has been shown that an atom between surface and tip can be transferred reversibly which results in bistable conductance. The controlled dynamics of adsorbed species has opened a new field of research. This thesis work provides a theoretical investigation of the controlled lateral and perpendicular motion of an inert gas atom (Xe) on metal surfaces.

The lateral motion of Xe on the Ni(110) and Pt(111) surfaces is manipulated by a W tip. The interaction energy of the physisorbed atom with the tip and metal surface is described by an empirical potential. Using molecular statics the energy surfaces are calculated and the adsorbtion sites are determined. By using the molecular dynamics calculations, the variation in the coordinates of the adsorbate Xe with the tip moving at a given height are obtained. Three different modes of Xe translation are distinguished depending on the height of the tip. These are i) carriage on the tip, ii) pushing and, iii) pulling modes. The range

of the tip height where one of these modes occur is strongly depended on the relaxation of electrodes and the geometry of the tip.

Controlled and reversible transfer of atoms between the metal surface and the tip is studied by the transfer of Xe between two flat Pt(111) surfaces. Physisorption of Xe on the Pt(111) surface is studied by an empirical potential including short and long-range interactions and yielding correct account of several experimental data. Effective charge on Xe and the dipole moment constructed therefrom are calculated as a function of the Xe-surface separation. The potential energy curve of Xe between two Pt(111) surfaces and quantum states of Xe therein are calculated as a function of the applied voltage and separation between two Pt(111) surfaces. Within this model, various mechanisms, such as tunneling of Xe, dipole excitation and resonant tunneling, electromigration contributing to the transfer of Xe are examined. The transfer rate of Xe is then calculated for different mechanisms. Its dependence on the bias voltage is explored. The overall behavior of the total transfer rate is not a power law. While at low bias voltages thermal assisted atom tunneling is effective, the dipole excitation and resonant tunneling becomes dominant at high bias voltages.

Keywords: Scanning tunneling microscope, atom transfer, atom switch, physisorption, chemisorption, Anderson-Newns model, molecular statics, molecular dynamics, inelastic electron tunneling, electromigration, dipole excitation, resonant tunneling.

Özet

ATOMLARIN METAL YÜZEYLERİNDE YATAY VE DÜŞEY YÖNDE KONTROLLÜ HAREKETLERİ

Alper Buldum
Fizik Yüksek Lisans
Tez Yöneticisi: Prof. Salim Çıracı
Kasım 1994

Geçenlerde bazı deneyler, tarama tünelleme mikroskobu (TTM) kullanılarak, metal yüzeylerinde bulunan atomların istenilen pozisyonlara taşınabileceğini gösterdi. Daha fazlası, bir atomun TTM'nin iki elektrodu arasında tersinir bir şekilde, kontrollü olarak hareket ettirilebileceği gösterildi ki bu durumda iki sabit iletkenlik değeri elde ediliyordu. Adsorbe olmuş atomların ya da moleküllerin kontrollü dinamiği yeni bir araştırma alanı açtı. Bu tez çalışması, bir asal gaz atomunun (Xe) metal yüzeylerinde, yatay ve düşey yönde kontrollü hareketlerinin teorik olarak incelenmesidir.

Xe atomunun Ni(110) ve Pt(111) yüzeylerinde yatay hareketleri Tungsten bir iğne tarafından sağlanıyor. Bu atomun iğne ve metal yüzeğiyle etkileşim enerjisi amprik bir potansiyelle ifade edildi. Moleküler statik metoduyla potansiyel enerji yüzeyleri hesaplandı ve adsorbsiyon pozisyonları tayin edildi. Moleküler dinamik metoduyla, verilen bir iğne yüksekliğinde Xe atomunun koordinatlarındaki değişiklikler elde edildi. İğne yüksekliğine bağlı olarak Xe atomunun üç çeşit hareketi keşfedildi: 1) İtilme 2) Çekilme 3) İğneye yapışarak taşınma.

Xe atomunun metal yüzeyi ile iğne arasındaki kontrollü ve tersinir hareketi

iki düzgün Pt(111) yüzeğiyle çalışıldı. Xe atomunun Pt(111) yüzeğiyle etkileşimi için kısa mesafe ve uzun mesafe etkileşimlerini içeren ve pek çok deneysel veriyle test edilmiş bir amprik potansiyel kullanıldı. Atomun efektif yükü ve metal yüzeyi ile arasında oluşan dipol momenti, atomla metal yüzeyi arasındaki mesafenin bir fonksiyonu olarak hesaplandı. Xe atomunun iki Pt(111) yüzeyi arasındaki potansiyel enerji eğrisi ve bu eğrinin özdeğerleri ve özfonksiyonları uygulanan voltajın ve iki elektrot arasındaki mesafenin bir fonksiyonu olarak hesaplandı. Bu modelin içinde, Zenon'un tünellemesi, dipol uyarılması ve rezonant tünelleme, elektrogöç gibi Xe atomunun geçişinde rol oynayan çeşitli mekanizmalar incelendi. Xe atomunun geçiş hızı çeşitli mekanizmalara göre hesaplandı. Bu hızın uygulanan voltaja nasıl bağlı olduğu keşfedildi. Toplam geçiş hızının genel davranışı akımın ya da voltajın üstel bir fonksiyonu şeklinde değil. Düşük voltajda sıcaklık destekli atom tünellemesi etkili iken yüksek voltajda dipol uyarılması ve rezonant tünelleme daha etkin oluyor.

Anahtar sözcükler: Tarama tünelleme mikroskobu, atom geçişi, atom anahtarı, tünelleme, fiziksel adsorbsiyon, kimyasal adsorbsiyon, Anderson Newns modeli, moleküler statik, moleküler dinamik, elastik olmayan elektron tünellemesi, elektrogöç, dipol uyarılması, rezonant tünelleme.

Acknowledgement

I would like to express my deepest gratitude to my supervisor Prof. Salim Çıracı not only for his invaluable guidence, efforts and encouragement but also for his academic personality as he is a model of a scientist for me.

I would like to thank Prof. Ş. Erkoç for his collaboration for lateral motion of Xe on the Ni(110) surface and for his support for molecular dynamics simulation technique.

I would like to thank Prof. W. A. Harrison for his invaluable discussions and remarks.

Lastly, I would like to thank A. K. Türkoğlu and my other friends for their moral support.

Contents

List of Figures

List of Tables

Chapter 1

INTRODUCTION

The article[1] titled "*Surface Studies by Scanning Tunneling Microscopy* " by Binnig, Rohrer, Gerber and Weibel opened a new era in surface physics in 1982. There was a description of a new device, *Scanning Tunneling Microscope* (STM), which was capable of real space imaging of surfaces with atomic resolution. It attracted great interest immediately and it spread out to the world in a short time. Nowadays, there are a large number of STM's in operation, in many fields of research, not only in surface physics but in chemistry and biology as well. After the invention of STM, many local probe methods were introduced. For example, Binnig, Quate and Gerber invented a new device, *Atomic Force Microscope* (AFM), which measured the force generated between the tip and the sample surface.[2]

STM is simply based on electron tunneling. A sharp tip is placed very close to the surface, to form a tunnel junction. This junction is very sensitive to the width of the tunnel barrier. The surface is scanned by the tip and hence by the tunneling current concentrated at the apex of the tip. This is the topography of the surface. The images correspond to local density of states at the Fermi level. Tersoff and Hamann developed a theory of STM.[3] They used Bardeen's transfer Hamiltonian formalism[4] to derive an expression for the current.

$$I = \frac{2\pi e}{\hbar} \sum_{\mu,\nu} f(E_\mu)[1 - f(E_\nu + eU)]|M_{\mu\nu}|^2 \delta(E_\mu - E_\nu) \qquad (1.1)$$

where $f(E)$ is the Fermi-Dirac distribution function. $M_{\mu\nu}$ is the tunneling matrix element between the states ψ_μ of the metal tip and ψ_ν of the sample surface:

$$M_{\mu\nu} = -\frac{\hbar^2}{2m}\int d\vec{s}(\psi_\mu^*\nabla\psi_\nu - \psi_\nu^*\nabla\psi_\mu) \tag{1.2}$$

E_μ and E_ν are the energies of the states in the absence of the tunneling and U is the sample bias voltage. This expression is simplified to read

$$I \propto \sum_\nu |\psi_\nu(\vec{r}_o)|^2\delta(E_\nu - E_f) \tag{1.3}$$

The right hand side is the surface local density of states (LDOS) at the Fermi level E_F at the position $\vec{r}_o$ of the point tip $\rho(E_F, \vec{r}_o)$. The tunneling current is not directly related to the position of atomic nuclei but related to the local density of states at the Fermi level. Tersoff-Hamann theory is valid for the tunneling between s-type states in the absence of significant tip-sample interaction effects. Another important application of STM is the surface spectroscopy where information on electronic surface states are derived from tunneling current vs. sample-bias voltage characteristics.

1.1 ATOMIC-SCALE MODIFICATIONS AND MANIPULATIONS

The STM has three main ingredients: atomically sharp tip, intense electric field and tunneling electrons. In addition to its main operation of surface imaging, it can deposit, remove and arrange surface atoms, affect the direction of magnetization, dissociate molecules, attach molecules to the substrates, detach molecules from substrates, induce phase transitions, enhance reactions, move atoms along the substrate and transfer atoms between the tip and substrate in a controlled way.[5] The experiments are performed at the close proximity of the tip in air, in ultra-high vacuum and also at a solid liquid interface. They provide valuable information about atomic and electronic structure, inter-atomic, intermolecular interactions, field effects and many other microscopic phenomena.

Surface modification on the atomic scale was first demonstrated by Becker et al.[6] They produced atomic scale hillocks on germanium surface by applying 4 volts bias on the tip. The Ge atoms on the tip were transferred to the sample so a field induced transfer of atomic species across the gap from the tip to the sample was realized. STM lithography was first done by Rigger et al.[7] and McCord et al.[8] Rigger scratched silicon surface with the tip touching to the surface. The pattern was a series of parallel lines in the hydrocarbon films covering the surface. Lyo and Avouris removed and redeposited individual Si atoms from Si(111) surface reducing the tip-sample distance.[9] Foster and Frommer described how to organize organic molecules on graphite surface[10,11] and studied the manipulation of individual molecules. They removed a molecule of phthalate by pulsing the tip with a 3.5 V threshold voltage. The STM was also used in the liquid environments such that GaAs surface was etched[12] in a $NaOH$, $EDTA$ solution and gold lines on p-type GaAs in a buffered solution of $KAu(CN)_2$ produced.[13]

An interesting usage of STM is for phase transitions . There is heating in the local scale by the electron beam from the STM tip where this heating is a function of thermal conductivity and the mean free path of electrons. In the crystalline materials the temperature rise is only a fraction of a degree but in amorphous materials heating by the tunneling electrons rise the temperature to higher values. Staufer et al.[14] examined the metallic glasses and formed a small pool of liquid under the tip. They increased the voltage to 2 volts and exceeded the melting temperature. Hydrogenated amorphous silicon is a material with low thermal conductivity and short mean free path. Jahanmir et al.[15] created lines by raising the temperature above the transition temperature and changed the film of amorphous silicon to crystalline state.

The storage of digital information is based on the polarization of magnetization in small magnetic domains. The STM with a magnetized tip could write on magnetic hard disks by changing local magnetization.[16,17]

Surface modification in the form of the creation of hillocks and craters was relatively clarified by Mamin, Guethner and Rugar with their work for atomic-emission from a gold tip to a gold substrate.[18] Gold atoms were emitted from the

tip in a controlled and reproducible way . They measured the threshold voltage for field-evaporation in close tip-sample separation and obtained $0.1V/\AA$ which is comparatively small with respect to $1V/\AA$ which is for the field to evaporate atoms from a tip in free space as in Field-Ion Microscope (FIM).[19] They proposed that the barrier height for field-evaporation was reduced by overlap of the atomic potentials when a metal surface was brought close to the tip.

Recently, Eigler and his collaborators performed two very important experiments, namely: i) Precise repositioning of an atom on metal surfaces.[20] ii) Controlled and reversible motion of an atom realizing atomic scale switch.[21] These experiments are very important because these were the first for controlling individual atoms like a child's play with a toy. This can take science and technology to a point that atomic scale devices can be produced or all the accumulated knowledge at a great library can be written in a few cm^2 area.The subject matter of this thesis is the theoretical investigation of these two experiments.

1.1.1 Positioning single atoms by STM

In the first experiment, Eigler and Scweizer[20] drag an atom over the surface from one location to another location without lifting the atom off the surface by carefully tuning the magnitude and direction of the tip force. The experiments were performed using an STM in an ultra-high-vacuum system and at $4K$. After dosing the Ni(110) surface with Xe, they took images as each Xe atom appears as a $1.6\AA$-high bump on the surface at random locations.The Xe $6s$ resonance, although lying close to the vacuum level, is the origin of the Fermi-level local state density which renders Xe visible in the STM.[22]

In figure 1.1, the steps for the controlled lateral motion of Xe are shown. (1) The atom is located and the tip is placed directly above it by operating the STM in the imaging mode. (2) The tip is lowered to a position where the atom-tip interaction is sufficient for the motion of the atom. This was achieved by changing the required tunneling current to a higher value in the range $1-6\times10^{-8}A$. (3,4)

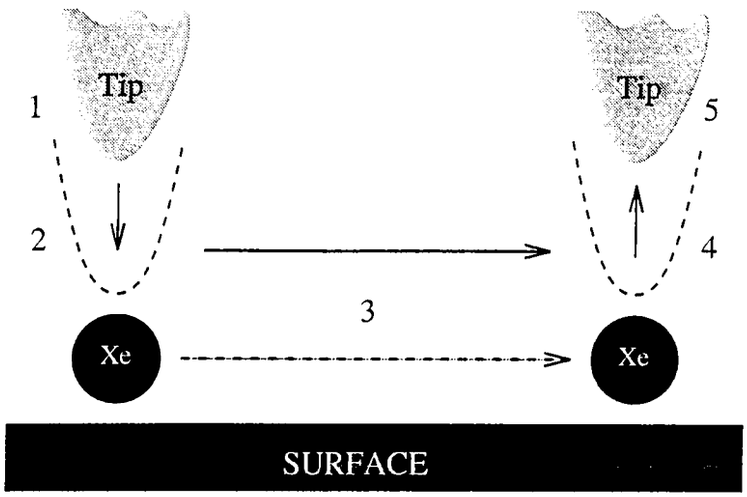

Figure 1.1: The process for sliding an atom across a surface
(1) The atom is located and the tip is placed directly above it. (2) The tip is lowered to a position where the atom-tip interaction is sufficient for the motion of the atom. (3,4) The tip is moved to a desired location, dragging the atom with it. (5) The tip is withdrawn to a position where the atom-tip interaction is negligible. The atom is left bound to the surface at the desired location.

The tip is moved to a desired location at a speed $4\mathring{A}$ per second, dragging the Xe with it. (5) Finally, the tip is withdrawn to a position where the atom-tip interaction is negligible. The Xe is left bound to the surface at the desired location.

The STM tip was produced from tungsten wire. The true chemical identity and the structure of the outermost atoms of the tip are not known yet. There was a threshold height below which the tip must be located to be able to move xenon atoms parallel to the rows of nickel atoms (the [110] direction of Ni(110) surface), and a lower threshold height to move perpendicular to the rows of nickel atoms (the [100] direction of Ni(110) surface) for any given tip and bias voltage. The magnitude and sign of the applied voltage had no significant effect on the threshold tip height. In figure 1.2 a linear multimer is shown which was produced by this process.

The Nickel (110) surface had an unreconstructed rectangular unit cell and the exact xenon periodicity of the xenon spacing was from the crystalline structure

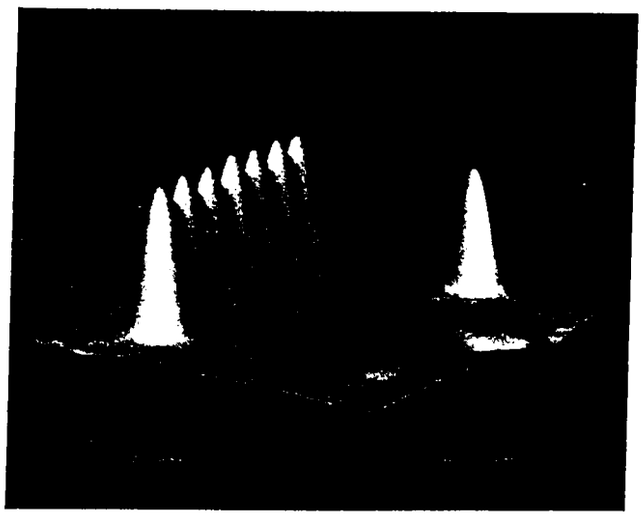

Figure 1.2: A linear chain of seven xenon atoms
A linear chain of seven xenon atoms bound to the Nickel (110) surface is shown. From reference 23.

of the underlying nickel surface. The xenon-xenon spacing along the row was uniform with $5.0 \pm 0.2\text{Å}$. This indicated that the xenon-nickel interaction dominates over the xenon-xenon interaction.

1.1.2 Atom Switch

The second important experiment is the creation of a bistable switch by Eigler, Lutz and Rudge. The switch derives its function from the motion of a single atom. This is an atomic-scale electronic device as called "*atom switch*". As the conduction electron wave functions decay exponentially in the tunnel barrier, the conductance of the STM's tunnel junction depends exponentially on the spacing between the electrodes. Slight rearrangements of the atoms in the current carrying region of the tunnel junction would lead to measurable changes in the conductance. The reversible motion of an atom between the surface and the tip of an STM becomes operation of a two terminal switch as in figure 1.3.

The switch was constructed using an STM in an ultra-high-vacuum system at $4K$. They slide the Xe atom like in the first process to a kink site along a

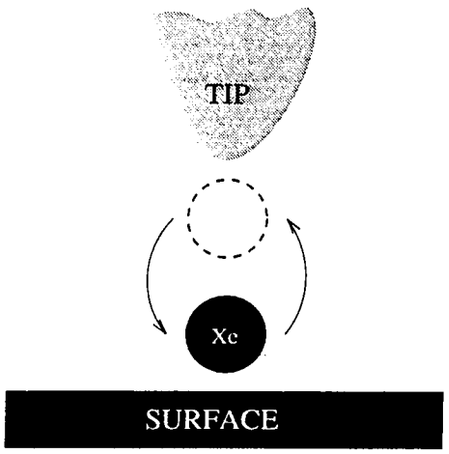

Figure 1.3: A two-terminal switch
The atom is reversibly transferred by applying a voltage pulse and the conductance of the tunnel junction changes according to the location of the atom.

monatomic step as it would enhance the probability that the Xe atom would bind to the same site whenever it is transferred to the surface. Then the feedback loop was turned off and the tip left at a fixed position above and $5\mathring{A}$ to the side of the Xe atom. The height of the tip was then adjusted to have a tunnel junction resistance of $1.5M\Omega$ with the tip biased at -0.02 volts with respect to the sample. During the operation of the switch, the STM was completely static. In figure 1.4 the time variation of the current during operation is displayed. It began with the Xe on the surface (A in figure 1.4) and the tip biased at -0.02 volts resulting in a $1.3 \times 10^{-8}A$ current. A $+0.8$ volt pulse is applied to the tip for 64 msec.Then the tip bias changed to -0.02 volts. (B is the voltage pulse in figure 1.4). The high conductance state of the switch was established by the pulse which have a resistance of $220K\Omega$. A -0.8 volt pulse was applied to toggle the switch back to its initial position for 64 msec, after which the bias was returned to -0.02 volts. (D is the voltage pulse in figure 1.4) The repetitions in figure 1.4 demonstrate the reproducibility of the switch toggling.

Eigler et al. took images during the operation of the switch and showed that Xe was on the surface at the low conductance state. At high conductance state, the Xe atom disapeared and the resolution of the atomic structure of the

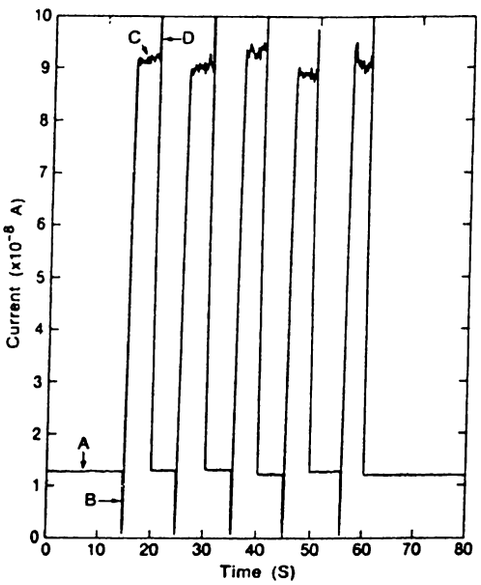

Figure 1.4: The time dependence of the current during operation of the switch. In the low-conductance state (A), the tip biased at −0.02 volts and the Xe bound to the surface. A +0.8 volt pulse is applied (B) to the tip for a duration of 64 msec after which the bias was turned to −0.02 volts. Thus, the Xe is transferred to the tip and the high-conductance state is established (C). A reverse −0.8 volt pulse is applied for 64 msec.(D) to reestablish the low- conductance state. From ref. 23

nickel surface was enhanced which shows that the tip structure and its electronic state were changed owing to the presence of the Xe atom on the tip. When they toggled the switch back to low conductance state, Xe again appeared on the surface showing the reversible motion. They found that the motion of the Xe atom was always towards the positively biased electrode (same direction with the tunneling electrons). Depending on the location of xenon on the surface, (i.e. kink site, terrace) the measured conductance ratios σ_s/σ_t varied from near unity to 7.

They measured a delay between the onset of the voltage pulse and the moment when the conductance changed due to the motion of the atom. Repeated measurements for a fixed tip-sample showed a simple randomness for the delay. The probability for the Xe atom remaining on the surface for a time t prior to transferring to the tip was fitted to the expression $P(t) = exp(-t/\tau)$ where the

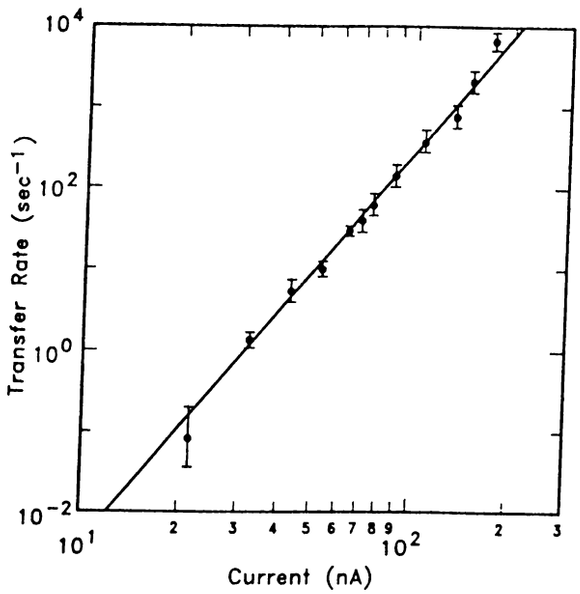

Figure 1.5: The transfer rate of a xenon atom
The transfer rate of a xenon atom from the Nickel(110) surface to the STM tip as a function of the current during the applied voltage pulse. From reference 23

characteristic time for the process τ was in good agreement with the mean delay. In figure 1.5 the transfer rate (the inverse of the mean delay) as a function of the current is shown. It is interpreted as a power law dependence upon the current as $I^{4.9\pm0.3}$. In order to better understand the controlled motion of atoms, brief information about forces in STM, physisorption and chemisorption of atoms on metal surfaces is given in next sections.

1.2 Forces in STM

The forces in STM due to the tip-sample interaction are crucial. They can derive atomic-scale modifications and manipulations. The sign and character of the tip force vary according to the value of the tip-sample separation z. At large z, it is attractive and Van der Waals force originating from the correlations between electronic fluctuations of the electrodes. This force is weak and uncorrugated

when the individual atoms are considered but may be large for the whole tip as it has a long range character. At small separations, the short-range force dominate the long-range VdW force. The short-range force have quantum-chemical origin and decay exponentially in the weak attractive region because of exponentially decaying wave-functions in the barrier.

For a better understanding the origin of the forces, Ciraci et al. calculated the interaction energy $E_i(z)$ between two rigid Al(001) slabs from self-consistent-field (SCF) calculations within the local density approximation[24] finding that $E_i(z)$ was strong but short ranged because the total energy of the tip-sample for a given separation was determined by charge-density overlap with only small deviations due to adhesive bond formation. Then they noted that for $z > z_e$, (z_e is the separation between the top-most layers of the two slabs where $E_i(z)$ is minimum.) $E_i(z)$ could be approximated by an exponential function. Rose et al. proposed a universal scaling relation in terms of the Rydberg function, $E_i^* = -(1+a^*)exp(-a^*)$ for the interaction energy versus distance dependence of metallic and covalently bound systems, including bulk crystals, parallel surfaces, adatoms diatomic molecules. In this expression, $E_i^* = E_i/E_b$, $a^* = (z - z_e)/\lambda$, and λ was taken proportional to the Thomas-Fermi screening length λ_{TH} or a fitting parameter either.

The short-range force on an individual atom j of the tip can be calculated from $\vec{F}_{s,j}(r) = -\nabla_i E_i(r)$. The perpendicular component $F_{s,\perp}(z)$ becomes increasingly attractive with decreasing separation, passes through a minimum, then decreases and becomes increasingly repulsive in the case of metals. There are weaker but significant lateral forces, smaller by one order of magnitude than the perpendicular forces as the vector contributions from all neighboring sample atoms tend to add up in $F_{s,\perp}$ but cancel out in $F_{s,\|}$.

The tip and sample atoms at small separation ($|\vec{r}| < 10\mathring{A}$) may have short range forces but the rest of the atoms further away have attraction due to VdW interaction. The interaction law $-C_n r^{-n}$ describes the VdW interaction energy at a distance r between the two atoms ($n = 6$)[25] , between an atom and polarizable flat surface ($n = 3$)[26] , or between two such surfaces ($n = 2$).[27] The laws in the

last two cases hold for the distances which are sufficiently large. In this case, details of the atomic structure are not important and a continuum description based on integration can be applied. C_n depends on the materials of the tip and sample and can differ significantly as the polarizability of a metallic tip and sample is larger than the sum of the atomic polarizabilities.[24] A generalized Lifshitz approach[28,29,47] can be applied to metal electrodes. It is expected to be valid at separations where the wave-function overlap and the exchange effects become negligible and remaining electron correlation effects require a non-local description. The forces in STM will be discussed in the next chapters in detail.

1.3 Physisorption and Chemisorption

1.3.1 Physisorption

If there is an attraction between a surface and an foreign atom or a molecule, it is called adsorption. It has the same basic forces that are known from the quantum of chemical bonding but now, one partner is a macroscopic medium with infinite number of electrons. Physisorption is the weakest form of adsorption where the contribution of the chemical bonding is marginal since the atom is hardly perturbed for adhesion. The origin of this bonding is the van der Waals interaction . The attraction here is due to the interaction of the polarizable solid with dipolar quantum mechanical fluctuations of the atomic charge distribution or in a simple way, the atomic electrons are attracted to their images in the solid.

A simple oscillator model of a physisorbed atom consisting of a positive ion and a valence electron is sufficient to understand the van der Waals interaction here.[30] The atom is located outside the surface at a distance z and r is the projection of the electron's orbital motion along the normal to the surface. The total electrostatic energy is

$$U(z) = \frac{1}{2}\left[-\frac{e^2}{2z} - \frac{e^2}{2(z-r)} + \frac{e^2}{2z-r} + \frac{e^2}{2z-r}\right] \tag{1.4}$$

Expanding equation 1.4 in powers of r/z,

$$U(z) = -\frac{1}{8}\frac{e^2r^2}{z^3} - \frac{3}{16}\frac{e^2}{z^4}r^3 + \cdots \tag{1.5}$$

The first (leading) term in equation 1.2 is proportional to the square of the oscillator and lowers the frequency of the atomic oscillator by an amount inversely proportional to the cube of the atom-surface separation. Usually one has:

$$V(z) = -\frac{C_V}{z^3} \tag{1.6}$$

The constant of proportionality C_V depends on the ability of the adsorbate and the substrate to polarize one another. The second term in equation 1.2 becomes important when the atoms is brought near to the surface. The ground state wave function φ_0 changes in first order to φ_0' in the perturbation theory and, $\langle\varphi_0'|\vec{r}|\varphi_0'\rangle \neq 0$ even though $\langle\varphi_0|\vec{r}|\varphi_0\rangle = 0$. The substrate induces a permanent dipole moment which increases as the atom approaches to the surface. There is a first-order correction to the interaction energy[29] and this correction defines the reference plane (the image plane) from which the van der Waals interaction should be measured.

$$V(z) = -\frac{C_V}{|z - z_V|^3} = -\frac{C_V}{z^3}(1 + \frac{3z_V}{z} + \cdots) \tag{1.7}$$

The electrons in the low density spill-out tail of the surface charge distribution begin to feel the presence of a nearby closed shell atom at short distances. Then the potential energy of the Bloch electrons is lowered by interaction with the atomic nuclear potential and the kinetic energy of these electrons is raised as their wavefunctions are orthogonalized to the atomic valence electron wave functions. At sufficiently short distances, repulsion wins. The total interaction energy is given in reference 30 as

$$V(z) = Kn(\vec{r}) - \frac{C_V}{|z - z_V|^3} \tag{1.8}$$

K is a constant and $n(\vec{r})$ is the ground state charge density of the surface. $n(\vec{r})$ decays exponentially into the vacuum so that physisorption potential has

a shallow minimum a few angstroms from the surface. At small separations, the first term of this equation can not give the repulsion correctly. This repulsion term must be an increasing function of separation due to core-core overlap and infinite at zero separation, but $n(\vec{r})$ is constant in the metal.

Although physisorption is described in terms of the van der Waals mechanism, Lang[31] demonstrated that the density functional formalism with local-density approximation for exchange-correlation described a variety of experimental measurements in such systems successfully. In this formalism with local-density approximation, the electron and its exchange-correlation hole are always attached. It differs from VdW mechanism in the degree of attachment. Lang proposed that, for equilibrium rare-gas-metal distances, the most important part of the valence-shell electron orbit (nearest to the metal) lies sufficiently within the surface electron gas so it is the most correct to consider the electron to be attached to the hole. An electron in the valence shell prefers to be on the metal side of the adatom rather then the vacuum side. In the VdW regime also, an electron prefers to be at the metal side to be closer to its own image. Thus a permanent dipole moment occurs in both cases, but the local-density approximation lacks the nonlocality included in the image interaction. Lang's calculations and charge density contour plots for Ar on $r_s = 3$ substrate ($\frac{3}{4}\pi r_s^3 \equiv \rho^{-1}$) and Xe on $r_s = 2$ substrate show dipole moments in a direction to decrease the substrate work function as experimentally predicted. The contour plots also show a resemblance to covalent bonding.

1.3.2 Chemisorption

Chemisorption is the chemical binding of an atom or a molecule to a solid surface. The binding energy is in the range of $\sim 1 - 2$ eV and is higher than the binding energy encountered in physisorption. Adsorbates usually include alkali metals, alkaline earths, and other metals, hydrogen, nitrogen, small inorganic molecules (CO, NO) and organics. The main adsorbents are the transition and noble metals and their compound, and diamond like semiconductors. Considering the single

atom chemisorption, there are three classes of theories.[32] The first class include simplified LCAO (linear combination of atomic orbitals) and Anderson model theories. The second class comprises first-principles self-consistent calculations. The third class consists of simplified theories based on electron correlation. The first class is dealt with throughout this subsection.

The tight-binding formulation of the chemisorption problem could contain an approximately orthonormal basis set consisting of the atomic orbitals $|i,\alpha\rangle$ belonging to the substrate atoms "i" and suitable atomic orbitals $|a,\beta\rangle$ of the adsorbate atom "a". The Anderson Hamiltonian[33] approach is used for the chemisorption problem.[34] The Anderson Hamiltonian is:

$$H_A = \epsilon_a^0 \sum_\sigma n_{a\sigma} + \sum_{k,\sigma} \epsilon_k n_{k,\sigma} + \sum_{k,\sigma} V_{ak}(c_{a\sigma}^+ c_{ak} + h.c) + U n_{a\sigma} n_{a-\sigma} \tag{1.9}$$

$c_{a\sigma}^+$ and $c_{a\sigma}$ are the Fermion creation operators for the electrons of spin σ in orbitals $|a\rangle$ and $|k\rangle$ respectively. $|k\rangle$ is the solid eigenstate and k is not a Bloch wavevector but an arbitrary notation. $n_{a\sigma}$ and $n_{k\sigma}$ are the number operators. The last term represents the Coulomb repulsion. This repulsion acts only between the electrons with opposite spin in $|a\rangle$. In the Hatree-Fock approximation, equation 1.9 is replaced by a one-electron Fock Hamiltonian H.[33]

$$H = \epsilon_a n_{a\sigma} + \sum_k \epsilon_k n_{k\sigma} + \sum_k V_{ak}(c_{a\sigma}^+ c_{a\sigma} + h.c) \tag{1.10}$$

Eigenvectors $|\varphi\rangle$ and eigenvalues ϵ_φ are introduced

$$H|\varphi\rangle = \epsilon_\varphi|\varphi\rangle \tag{1.11}$$

and $|n\rangle$ are expanded in terms of $|a\rangle$ and $|k\rangle$.

$$|\varphi\rangle = |a\rangle\langle a|\varphi\rangle + \sum_k |k\rangle\langle k|\varphi\rangle \tag{1.12}$$

The density of states localized in the adatom orbital is

$$\rho_a(\epsilon) = \sum_\varphi |\langle\varphi|a\rangle|^2 \delta(\epsilon - \epsilon_\varphi) \tag{1.13}$$

which can be formulated as[34]

$$\rho_a(\epsilon) = \pi^{-1}\Delta/[(\epsilon - \epsilon_a - \Lambda)^2 + \Delta^2] \tag{1.14}$$

with

$$\Delta(\epsilon) = \pi \sum_k |V_{ak}|^2 \delta(\epsilon - \epsilon_k) \tag{1.15}$$

and

$$\Lambda(\epsilon) = P \sum_k \frac{|V_{ak}|^2}{\epsilon - \epsilon_k} \tag{1.16}$$

P is the Cauchy Principle Value.

The function $\rho_a(\epsilon)$ is reminiscent of a Lorentzian function and when the energy dependence of Δ and Λ is neglected, it becomes exactly a Lorentzian function with a single peak of width $\sim 2\Delta$, centered at the energy $\epsilon = \epsilon_a + \Lambda$. This limiting case of the Anderson model is called as *virtual state* by Newns and Muscat.[32] In this case, the adatom energy level is shifted by Λ, subject to a lifetime broadening Δ, but still remains its identity.

In the next chapter, we study the controlled lateral motion of Xe on the Ni(110) and Pt(111) surfaces by using molecular statics and dynamics methods. In chapter 3 we study the controlled and reversible transfer atoms between the metal surface and tip by the transfer of Xe between two flat Pt(111) surfaces. We consider various mechanisms contributing to the transfer of Xe. Finally, in chapter 4 we summarize our conclusions.

Chapter 2

CONTROLLED LATERAL MOTION OF Xe

Eigler and Schweizer demonstrated that individual atoms which are physisorbed on metal surfaces can be controlled and relocated by using a Scanning Tunneling Microscope. They transfered Xe atoms physisorbed on Ni(110) surface to desired positions by a W(111) tip. Their experiment showed that manipulation of surfaces, clusters and molecules by controlling atoms one by one is not a dream any more. However, there are still many things we do not know about controlled motion of atoms. The effect of tip induced modifications, the role of structural and material parameters are crucial and require further investigation. This chapter presents the theoretical study for the lateral translation of Xe on metal surfaces. In the first section, controlled lateral motion of Xe atom on Ni(110) is studied using molecular statics and dynamics methods. The interaction between atoms are represented by a Lennard-Jones type two-body empirical potential. The objective here is not performing the simulation of Eigler's experiment but having a further understanding of the phenomena. In the second section controlled lateral motion of Xe on Pt(111) is studied. The interaction between Xe and the Pt(111) surface is represented by a more elaborate empirical potential.

2.1 Xe Motion on the Ni(110) Surface

2.1.1 Interaction Potential and Atomic Model

The interaction between the adatom and the metal surface has three components at very low temperatures. These are (i) chemical interaction due to charge rearrangement; (ii) the repulsive interaction due to the Pauli Exclusion Principle; (iii) the weak Van der Waals interaction. For noble gas atoms like Ar or Xe, the charge rearrangement is small so the chemical interaction is weak. The repulsion interaction becomes significant when the atom is closer to the surface then the equilibrium distance d_o. The interaction energy is in the range of $150 - 400$ meV. Ciraci et al. calculated the binding energy of the Xe adsorbed on the Al(100) surface and had $\sim$ 130 meV by the self -consistent psuedopotential calculation method.[35] This binding energy includes repulsive and chemical interaction with the exchange correlation energy obtained in the local density approximation. While the experimental binding energy[36] is approximately 200 meV, the LDA binding energy is well comparable to the Van der Walls binding energy. It is hence concluded that the charge rearrangement in many physical phenomena has to be considered.

In condensed matter systems we usually have many degrees of freedom. For interactions in many-body systems, it is useful for one to integrate out a number of degrees of freedom to obtain effective interactions which are still at microscopic scale and show the basic physics. These effective interactions are usually obtained by a low-order expansion in powers of one or more bare interactions.[37] For the total configurational energy of a condensed matter system, the simplest type of description is

$$E_c = \frac{1}{2!}\sum_{i,j} V_2(\vec{R}_i, \vec{R}_j) + \frac{1}{3!}\sum_{i,j,k} V_3(\vec{R}_i, \vec{R}_j, \vec{R}_k) + \cdots \tag{2.1}$$

where E_c is the configurational energy of the solid and V_n are the interatomic potential functions of n^{th} degree.

The interaction between the Xe atom and the metal surface is represented by empirical two-body interaction potential to perform molecular statics and

Interaction	$\epsilon(eV)$	$r_o(\text{Å})$	C_b	C
Xe-Ni	0.218	3.27		0.15658
Xe-W	0.339	3.62		0.14829
Ni-Ni	2.07	2.56	0.128034	
W-W	5.00	2.82	0.112344	
Ni-W	0.38584	2.69	1.000000	

Table 2.1: Energy parameters for two body Lennard-Jones potential

dynamics calculations. This two-body interaction potential between an electrode atom i ($i = t$ tip; $i = s$ substrate) and the adatom a is Lennard-Jones type.

$$U_{ia}(|\vec{r} - \vec{R}_l|) = \epsilon \left[\left\{ \frac{|\vec{r} - \vec{R}_l|}{r_o} \right\}^{12} - 2 \left\{ \frac{|\vec{r} - \vec{R}_l|}{r_o} \right\}^{6} \right] \tag{2.2}$$

For the controlled lateral translation of the adatom, the total potential energy is

$$U(\vec{r}, \ldots, \vec{R}_l, \ldots \vec{T}_m) = C \sum_l U_{sa}(|\vec{r} - \vec{R}_l|) + C \sum_m U_{ta}(|\vec{r} - \vec{T}_m|) +$$
$$C_b \sum_{l>m} U_{ss}(|\vec{R}_l - \vec{R}_m|) + C_b \sum_{n>m} U_{tt}(|\vec{T}_n - \vec{T}_m|) + C_b \sum_{l,n} U_{st}(|\vec{R}_l - \vec{T}_n|) \tag{2.3}$$

$\vec{R}_l$ and $\vec{T}_m$ are the position vectors of metal surface and tip respectively. The constants C and C_b are the scaling factors to take into account the many-body effects for surface (U_{ia}) and bulk (U_{ii}) pair potentials. The interaction energy is equal to the experimentally measured heat of adsorption of the adatom. The heat of adsorption of Xe atom and its height on various surfaces have been determined experimentally.[38,39] The pair potential parameters ϵ and r_o of U_{ia} are determined by fitting the calculated heat of adsorption and the optimum height of Xe on the corresponding surface . The pair potential parameters for Ni-Ni, W-W and Xe-Xe are available in the literature.[40,41] The parameters used in the calculations are given in table 2.1.

A better interpretation of the interaction between Xe and the electrodes may include additional term beyond the central force term. Short-range (chemical)

interaction can be better presented by an exponential term. Especially, the effective potentials having minimum energy on top side include non-central terms. The potential described by equation 2.3 has been used in the calculation because of limited number of experimental data available to fit the parameters therein. For the calculations with the rigid tip and sample, the positions of electrode atoms $\vec{R_l}$ and $\vec{T_m}$ are kept fixed in their ideal bulk positions and the terms U_{ss} and U_{tt} in equation 2.3 are omitted. The substrate is represented by 12716 Ni atoms in 34 layers. Each layer contains 374 atoms (22×17) . The tip is constructed by 2027 W atoms in pyramidal geometry generated from W(111) surface containing 22 layers. In the calculations with relaxed electrodes, we used relatively smaller electrodes comprising number of atoms treated with the periodic boundary condition. The substrate has 3750 Ni atoms in 10 layers each containing 375 atoms (25×15). In figure 2.1 the model is shown schematicaly. The first five layer of the tip and the first two layer of the sample is shown in the upper scheme with the xenon as a dark filled circle. In the lower scheme xenon on the sample at the minimum energy position is shown with the lattice vectors and the corresponding directions. ($[1\bar{1}0]$ is chosen as the x direction and [100] is chosen as the y direction.)

2.1.2 Molecular Statics

Having decided the effective pair potential, we next analyze the energy variation of the Xe atom on the bare sample surface due to its location, and we search surface for the energy topography. This analysis is performed by calculating the potential energy surface. All the atoms of the sample are kept fixed at their ideal positions and the surface is turned into a 2D grid. $U(\vec{r})$ is minimized by varying the height of the xenon atom at each grid point (x, y) on the surface. Figure 2.2(a) is the calculated potential energy surface and it indicates that Xe is physisorbed at the hollow (H) site of the ideal Ni(110) surface. The energy barrier Q_L across the long bridge site (L) is lower than that Q_S across the short bridge site. The energetics obtained are outlined in 2.2. Binding site of the Xe atom is still controversial. The present and earlier calculations calculations agree

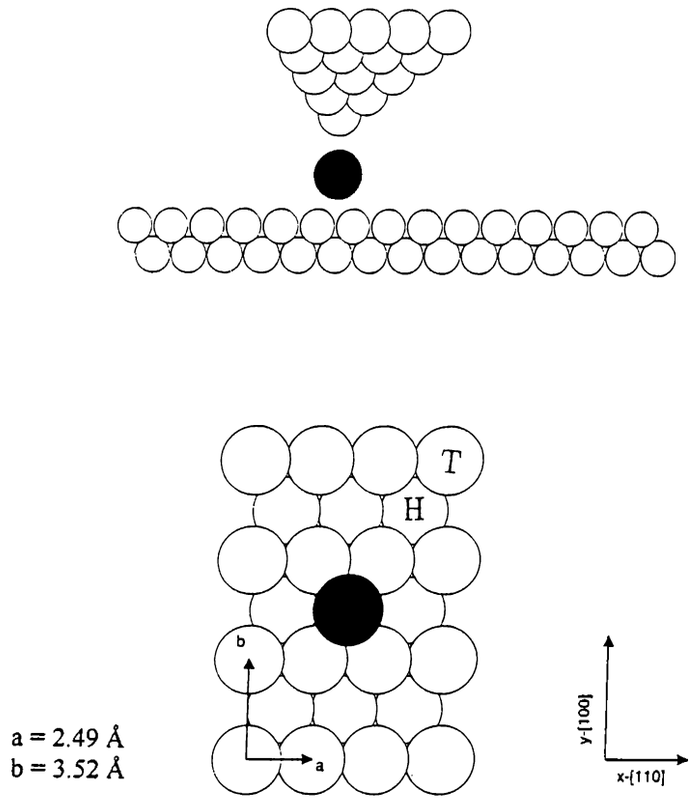

Figure 2.1: Schematic representation of the model
In the upper scheme, the first five layer of the tip and the first two layer of the sample is shown with the xenon as a dark filled circle. In the lower scheme xenon on the sample at the minimum energy position is shown with the lattice vectors and the corresponding directions.

on the H-site[42] but the top site has also been proposed.[43,44] In figure 2.2(b) the energy of the Xe atom on the bare W(111) tip is shown. The energy is highest when Xe lies above the apex atom but become lowest at the three hollow site between the apex and the second layer atoms. The binding site is the hollow site corresponding to the center of the triangle between the apex and second layer atoms. In figure 2.2(c) the total potential energy of Xe on the Ni(110) surface with a W(111) tip lying 5.0$\AA$ above the surface is shown. The apex of the tip is above the hollow site of the surface so the variation of the Xe energy on the bare surface reflects itself as having two peaks. A single peak occurs when the tip apex is above the top site of the surface.

The energy minimum of the Xe atom depends directly on the tip position.

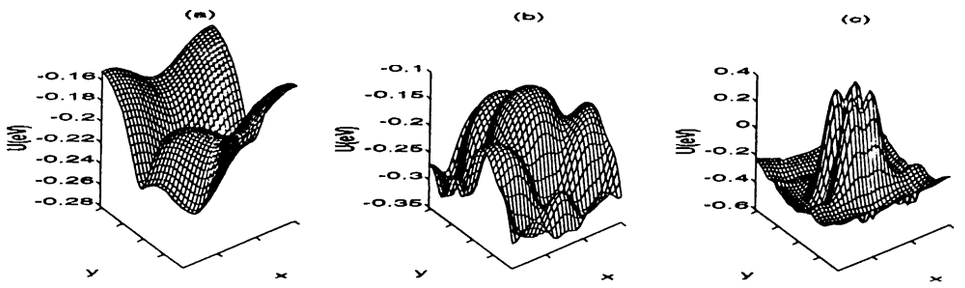

Figure 2.2: Potential energy surfaces
(a) The potential energy of Xe on the Ni(110) surface (b) Same for Xe on the W(111) tip (c) The total potential energy of Xe on the Ni(110) surface with a W(111) tip lying 5.0$\mathring{A}$ above the surface. The plot covers (3×3) cell of the Ni(110) surface.

Binding Energy	E_b (meV)	Barrier Energy	Q (meV)
H-site	280	H→S→H	102
T-site	151	H→L→H	46
L-site	234	H→T→H	129
S-site	178		

Table 2.2: Energetics of Xe on the Ni(110) surface

The magnitude and the position of the energy minimum vary with the changes of the tip position. In figure 2.3, the variation of the minimum potential energy U and corresponding height h of Xe for different positions of the tip is shown. The height of the tip apex is kept fixed 5.0$\mathring{A}$ and 5.4$\mathring{A}$ above the Ni(110) surface and Xe position is varied on the [100] line bisecting the unit cell at each scheme. The calculations are repeated for different tip positions on the [100] line. The minima of the potential energy curves are the possible position of the Xe atom as it is pulled or pushed by the W(111) tip. Changes in magnitude and position of this minima can be seen, and these changes may give the picture of how Xe is changing its position. The height h versus the coordinate κ of the Xe atom indicates that, in some cases, the potential energy is lowered if Xe is attached to the tip.

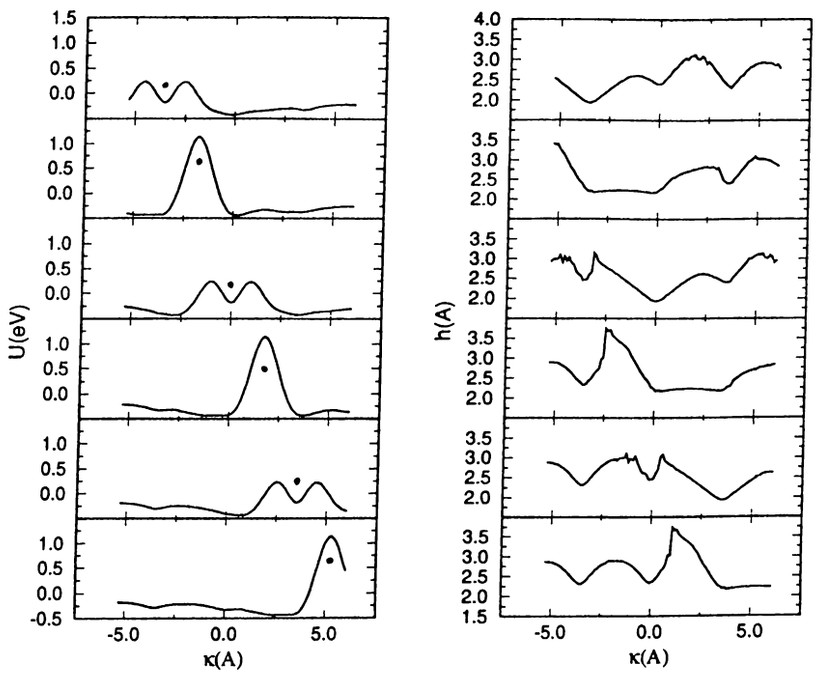

Figure 2.3: Variation of minimum energy U and height h of Xe
Variation of minimum energy U and height h of Xe for different position of the tip on the Ni(110) surface. The tip moves 5.$\AA$ above the Ni(110) atomic plane on the [100] line bisecting the unit cell. The position of the tip in each panel is marked by a dot.

2.1.3 Controlled Lateral Translation: Dynamics

Understanding the dynamical behavior of the Xe needs further analysis than calculating the potential energy surfaces and searching the minima. Does the Xe atom always go to the nearest local minima or have a more complex behavior due to its kinetic energy ? To answer this question for the carriage of Xe on the Ni(110) surface, the method of molecular dynamics computer simulation is applied. Computer simulation is a test of theories by performing experiments not in the real manner but in computer media. Molecular Dynamics (MD) is the term used to describe the solution of the classical equations of motion (Newton's equations) for a set of molecules.[46]

In MD simulations, the time increments must be small in order to capture adiabaticity. For the lateral translation of Xe the time steps are $\delta t = 1.0 \times 10^{-14}$ –

$1.0 \times 10^{-15}s$. The tip is moved with a constant speed $v_t = 5.28 \times 10^{10}\mathring{A}/s$ in [100] (y) direction and $v_t = 3.74 \times 10^{10}\mathring{A}/s$ in $[1\bar{1}0]$ (x) direction. Apparently, this speed is much larger then the speed in the experiment ($4\mathring{A}/s$) but it is affordable only with the available computer capacity. Nevertheless, v_t is much smaller than the sound velocity in the metals so phonon propagation is much faster. Initially the Xe is placed at the hollow site on the surface; the tip initially behind the Xe atom is moved along a line passing on the Xe atom at a constant height. Figure 2.4(a) represents the results related to the motion along the [100] direction (or y direction). The Xe atom is practically not affected by the tip for heights $h_t \geq 5.6\mathring{A}$ above the Ni(110) atomic plane. (The height of Xe at equilibrium is $2.3\mathring{A}$) On the other hand, the Xe atom is attached to the tip at $h_t = 5.4 - 5.5\mathring{A}$. This is specified as the contamination of the tip by Xe. For $h_t < 5.4\mathring{A}$, Xe moves behind the tip and experiences periodic jumps across the long bridge. This corresponds to the pulling mode of the lateral translation. It is interesting to note that for $h_t \leq 4.8\mathring{A}$ the Xe atom is attracted so much that the atom first jumps backwards then follows the tip. The contamination and pulling mode of lateral translation are clearly shown in figure 2.4(b) which shows the real space trajectory of Xe in $y - z$ plane. ($\kappa - \zeta$ respectively)

Lateral translation of Xe induced by the motion of the tip along the $[1\bar{1}0]$ direction is also studied. The motion occurs in a line across the short bridge. Two different modes are found in the motion along this direction. Pulling and pushing modes depend on the tip height. As it can be seen in figure 2.5(a); the Xe atom is pulled by the tip at $5.8 \geq h_t \geq 5.4\mathring{A}$ and pushed at $h_t \leq 5.3\mathring{A}$. The coordinate of the Xe atom along x direction is denoted by ξ. Eigler obtained a threshold height for the motion parallel to the rows of the atoms on the Ni(110) surface ($[1\bar{1}0]$ direction) and a lower threshold height for the motion perpendicular to the rows of the atoms ([100] direction). Here the threshold height for the $[1\bar{1}0]$ direction is $5.8\mathring{A}$ and for the [100] direction is $5.4\mathring{A}$ which are consistent with the experiment. If the tip moves along the body-diagonal of the surface unit cell (or [112] direction) the Xe atom performs zig-zag motion as seen in figure 2.5(b). The jump along the [100] direction is followed by the jump along the $[1\bar{1}0]$ direction

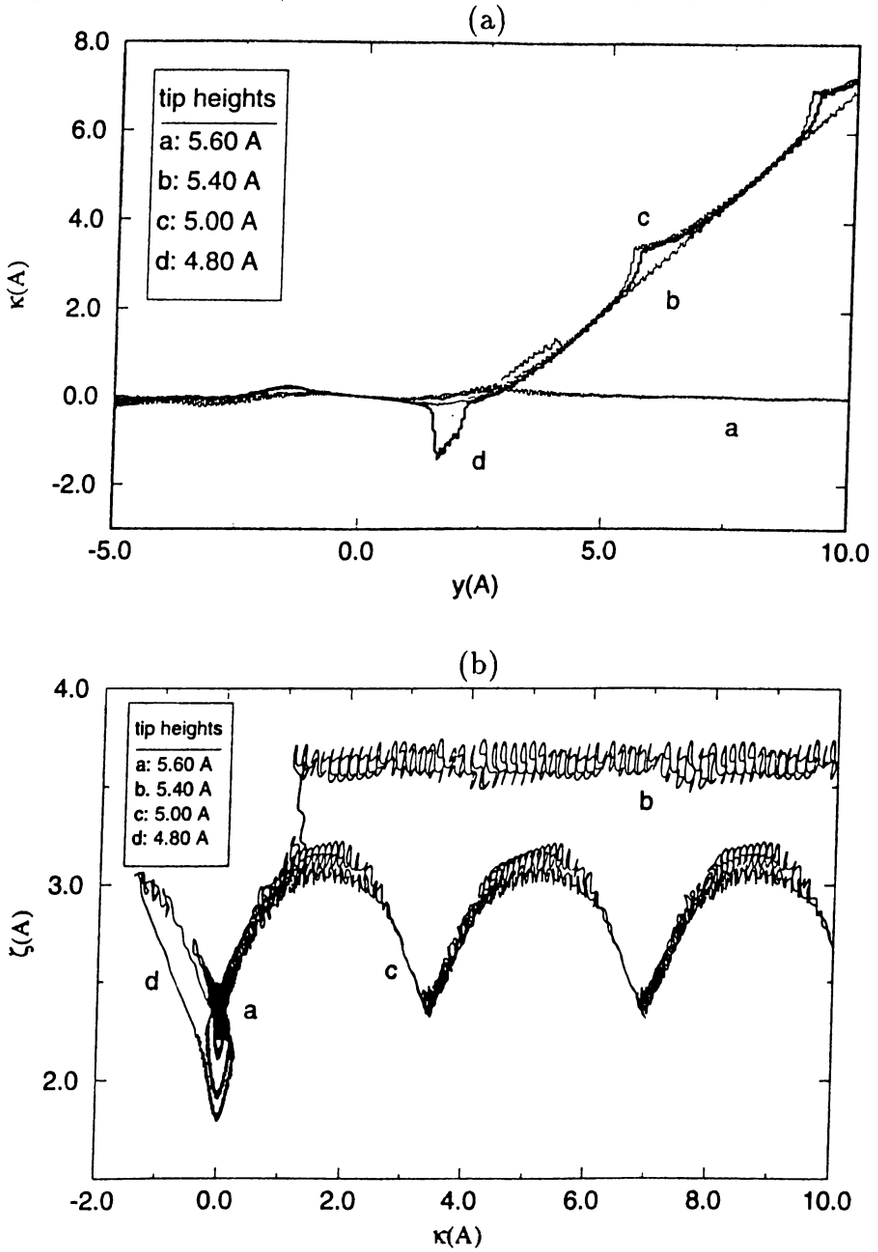

Figure 2.4: Lateral translation of Xe along the [100] direction (a) Lateral translation of the Xe atom induced by the moving tip along the [100] direction with different tip heights above the Ni(110) surface. y and κ are the coordinates of the tip and Xe along the [100] direction, respectively. (b) The variation of height ζ of the Xe atom during lateral translation along the [100] direction.

thus zig-zags of $\kappa(\xi)$ are quite sharp. However, for small height ($h_t = 5.\mathring{A}$) the zig-zags are not sharp owing to the increased tip-adatom interaction.

In figure 2.6, the forces due to tip and sample on Xe are shown for the tip

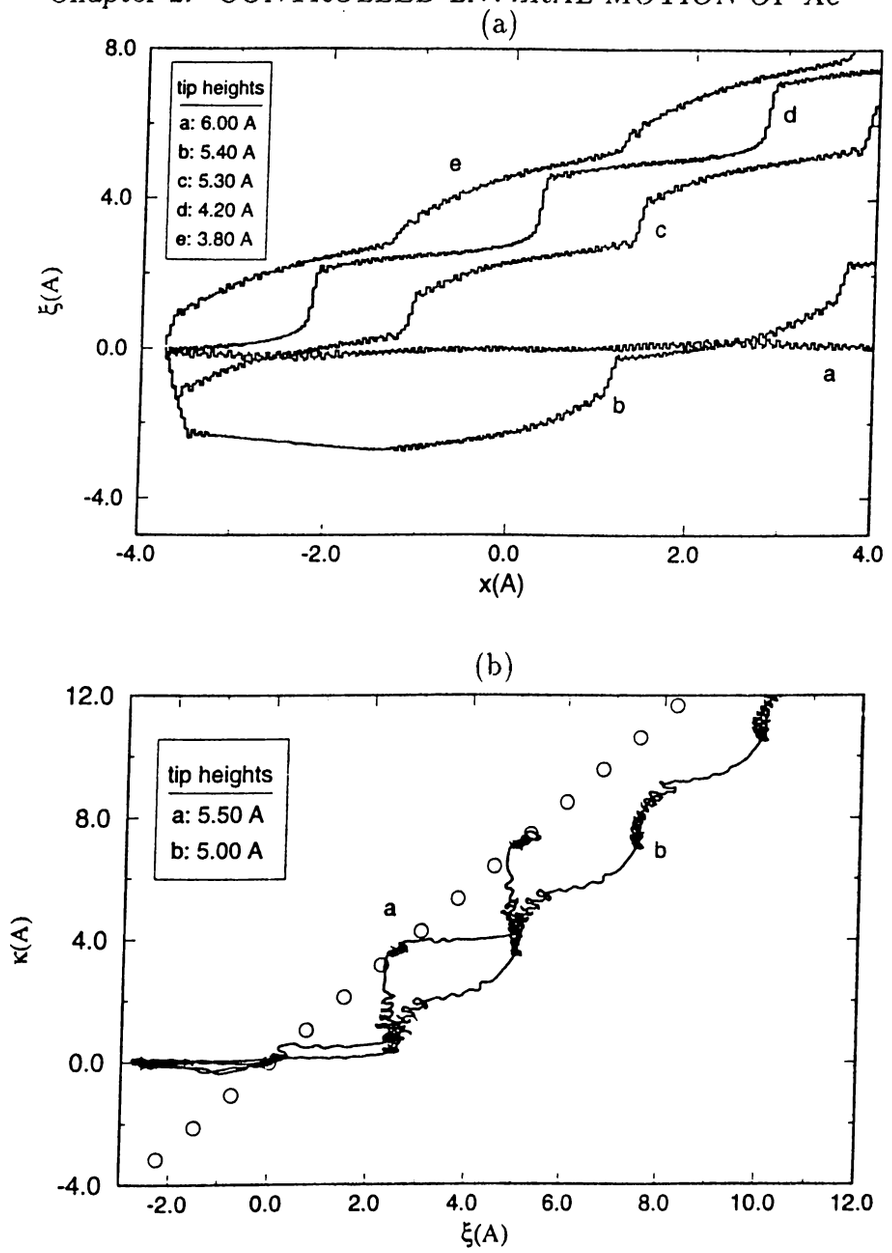

Figure 2.5: Lateral translation of Xe along $[1\bar{1}0]$ direction and [112] direction (a). Lateral translation of the Xe atom induced by the moving tip along the $[1\bar{1}0]$ direction with different tip heights above the Ni(110) surface. (b) Lateral translation of Xe along the [112] direction

height $h_t = 5.\mathring{A}$. First two panels show the variation of Xe κ, ζ coordinates with tip's y coordinate. Third panel shows the forces due to tip and sample on Xe in y direction. Forth panel shows the forces on Xe in z direction; and fifth one is the panel which shows the total force on Xe along y direction. Last panel is the

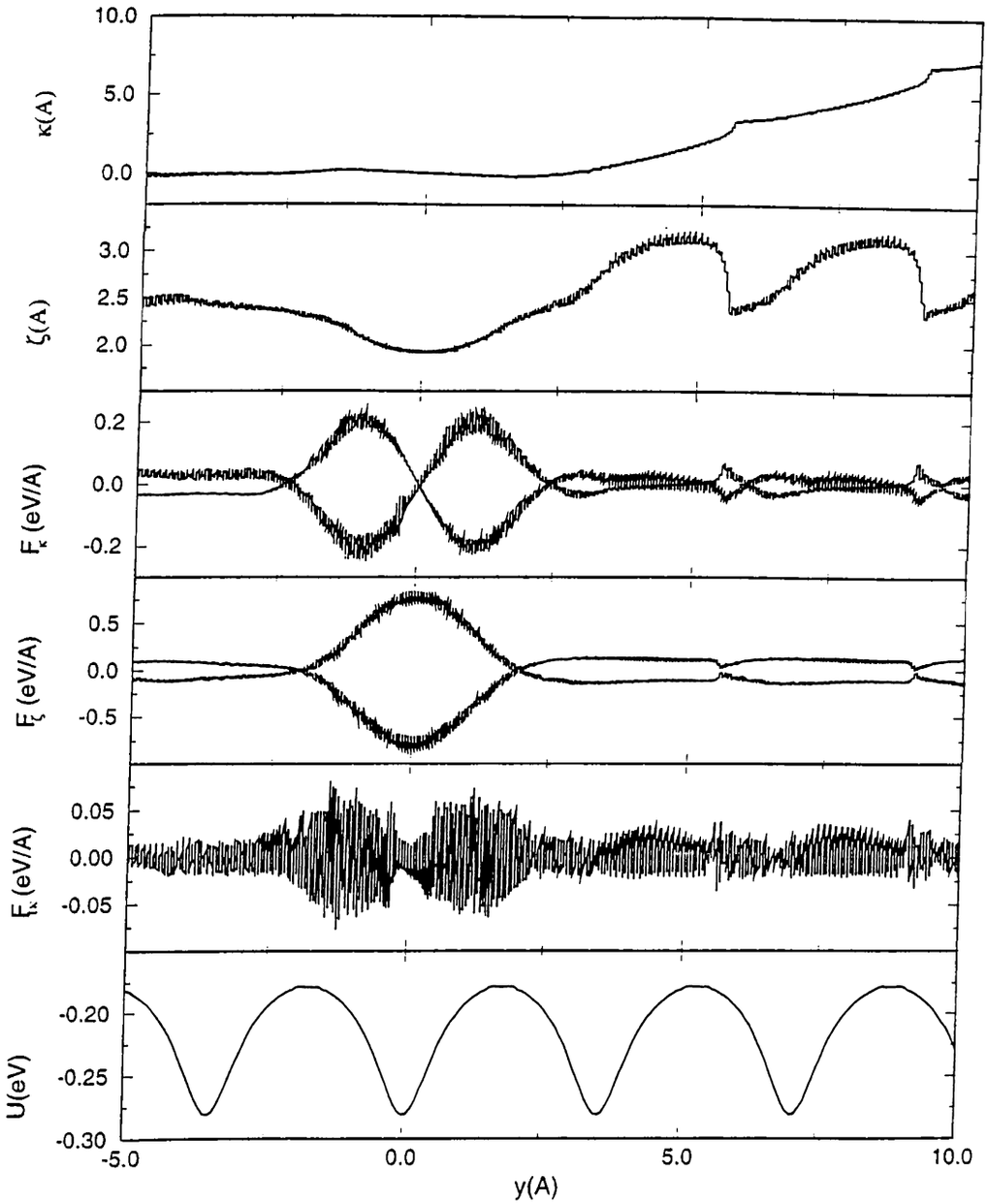

Figure 2.6: Forces on the Xe atom for $h_t = 5.\mathring{A}$

Variation of lateral coordinate κ and height ζ of Xe, components of forces on the Xe atom exerted by the sample and the tip, variation of potential with the y-coordinate of the tip moving at constant height $h_t = 5.\mathring{A}$

plot for the potential. For all panels, horizontal axis shows the tip coordinate in y direction. The tip force is first attractive then follows the sequence repulsive-repulsive-attractive. The sample force is always in the reverse direction of the tip force.

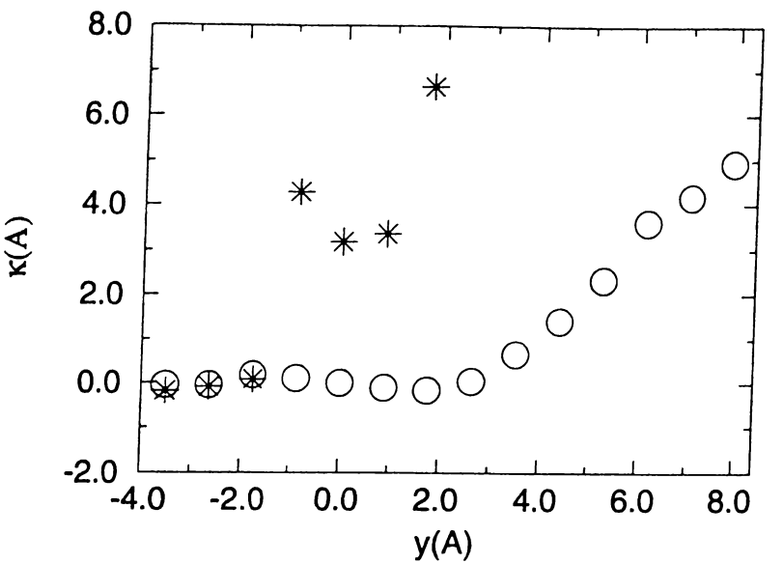

Figure 2.7: Lateral translation of Xe in the case of relaxed electrodes Displacement of κ of Xe versus displacement of y of the tip along the [100] direction bisecting the surface unit cell. Circles and stars corresponds to the rigid and relaxed electrodes, respectively.

The relaxation of electrodes becomes important for small h_t where the force $F_{t,s}$ on Xe is exerted by a small number of atoms of the sample and of the close proximity of the tip. In this case, the values of Q_L and Q_S are modified. The relaxation is considered by including all the terms in equation 2.3 and by allowing all the atoms at the close proximity of the tip to move under the action of the force by the rest of the system. In our calculation, first two layers of the sample ($2 \times 375 = 750$) atoms and first five layers of the tip (35) atoms are allowed to move together with Xe. The parameters of the empirical potential for $t - t$ and $s - s$ interactions are obtained from the experimental data, whereas the parameters related with $t - s$ interaction are determined by averaging those of bulk Ni and W. As the tip and the sample atoms start to move around their equilibrium positions, the fluctuations on the value of the force acting on Xe are changed. These changes may cause important differences on the translation of Xe with rigid electrodes. Figure 2.8 shows the important effect of the electrode relaxation . At the end of each step displacing the tip by $0.88\mathring{A}$, the molecular dynamics calculation are carried out taking initial conditions as the resulting

conditions of the previous step. While the Xe atom is only pulled by the rigid tip at $h_t = 5.0\mathring{A}$, in the case of relaxed electrodes, the motion proceeds in the pushing mode. Another important effect of relaxation is that in certain conditions the Xe atom starts to escape sideways. The sideways motion was absent in the case of rigid electrodes since the resultant lateral force perpendicular to the direction of motion has vanished.

2.2 Xe Motion on the Pt(111) Surface

2.2.1 Interaction Potential and Atomic Model

As in the previous case, the interaction energy between Xe and the Pt(111) surface is composed from: 1) Short-range attractive interaction due to the chemical bond between Xe and the Pt(111) surface. (This interaction includes electrostatic, exchange and correlation energies.) 2) Short-range repulsive energy 3) Long-range Van der Waals energy. For closed-shell atoms, such as Ar and Xe, the charge rearrangement upon physisorption on metal surface was thought to be negligible. Reviewing the experimental information available from work function measurements and electron spectroscopies concerning the adsorption of rare gases on metal surfaces, Ishi and Viswanathan concluded that chemical bonding effects play a significant role in Xe adsorption.[45] Barker and Rettner determined an empirical potential energy function for the interaction of xenon with the Pt(111) surface[43] This function describes a wide range of dynamical and equilibrium experimental data including scattering measurements, with detailed angular distributions and energy transfer data. They also used thermal desorption rates and trapping probabilities, as well as thermodynamic properties of monolayer phases. The potential also agrees with an experimental value for the frequency of vibration normal to the surface, and has the correct asymptotic behaviour at large distances from the surface. ($V = -c_3/z^3$, with an experimental estimation of c_3) The equilibrium position for a single Xe atom lies directly above the surface platinum atom of a height of $3.35\mathring{A}$.

Barker and Rettner represent the interaction between a single Xe atom and the solid by a sum of nonspherical pairwise additive potentials, together with an additional term V which depends only on the normal distance z_g^{av} of the xenon atom from the local surface and describes the interaction with the delocalized conduction electrons. They modeled the nonspherical pair potential by a spherical part centered on the Pt atom, a function of the distance R_{gi} between the Xe atom and the ith Pt atom, and a part centered a distance h above the Pt atom, a function of R'_{gi}, where

$$R'_{gi} = (x_g - x_i)^2 + (y_g - y_i)^2 + (z_g - z_i - h)^2 \tag{2.4}$$

The total energy of the xenon on Pt(111) surface is given by

$$U = \sum_i [u(R_{gi}) + v(R'_{gi})] + V(z_g^{av}) \tag{2.5}$$

The spherical function $u(R)$ has the form

$$u(R) = A_2 exp(-\alpha_2 R) \tag{2.6}$$

They define a function F by

$$F(C, \gamma, E; z) = ECexp(-\gamma z)/[E + Cexp(-\gamma z)] \tag{2.7}$$

v and V are given in terms of this function.

$$v(R') = F(A, \alpha, W; R') - c_6 G(R')/R'^6 \tag{2.8}$$

$$V(z) = F(A_1, \alpha_1, W_1; z) \tag{2.9}$$

where the damping function is defined by

$$G(R) = 1, \ R > R_1 \tag{2.10}$$

and

$$G(R) = exp[-(R_1/R - 1)^2], \ R \leq R_1 \tag{2.11}$$

They found an optimized *on-top potential* (potential with minima over the on-top site) which gave a very good description of the whole body of data. The parameters for this potential are given at table 2.3.

A_1	3.196×10^4 eV	A_2	5.926×10^9 eV	C_6	82.72 ev $\mathring{A}^6$
α_1	4.25 $\mathring{A}^{-1}$	α_2	9.00 $\mathring{A}^{-1}$	h	1.83 $\mathring{A}$
W_1	1.0 eV	δ	0.22 $\mathring{A}^{-2}$	R_1	6.8247 $\mathring{A}$

Table 2.3: Parameters for On-Top potential

The interaction potential between xenon and the atoms of the W tip is taken from earlier calculation and is expressed in terms of a pair potential of Lennard Jones type. The parameters ϵ and r_o are the same with the parameters in subsection 2.1.1 . The sample is represented by 14112 Pt atoms in 42 layers. Each layer contains 336 atoms (21×16). The atomic structure of the tip is the same as the tip generated from W(111) surface in the previous section. It is constructed by 2024 W atoms in pyramidal geometry containing 22 layers. There is a single atom at the apex of the tip and second layer has three atoms.

2.2.2 Potential Energy Surfaces

In order to analyze the motion on Xe, we first obtain the potential energy surface which is the surface topography for the energy of the Xe atom. Like Xe on the Ni(110) surface in the previous section, a 2D grid of the Pt(111) surface is formed. $U(r)$ is minimized at each grid point (ξ, κ on the surface by varying the height ζ of the Xe atom. Figure 2.9(a) shows the potential energy surface for Xe on bare Pt(111) surface. The lowest value of potential energy is -0.2540 eV and occured at the top sites. Thus, the calculated equilibrium position of xenon atoms physisorbed on the Pt(111) surface is located on top of the platinum atoms. The energetics of Xe on the Pt(111) surface are given in table 2.4. The equilibrium site for rare gas atoms physisorbed on metal surfaces were usually predicted as the hollow site; the top found in this case seems to be at variance with earlier findings. The d-band electrons in transition metals is pointed out to give rise to a different adsorption site.[47] Müller has performed a local density functional calculation of the interaction energy of Xe with a rigid Pt cluster representing

Binding Energy	E_b (meV)	Barrier Energy	Q (meV)
H-site	222	T→H→T	31.53
T-site	254	T→B→T	26.39
B-site	228		

Table 2.4: Energetics of Xe on the Pt(111) surface

the (111) surface.[44] This calculation also has predicted that the equilibrium site is above the on-top site due to charge transfer from the Xe $5p$ orbital to empty $5d$ orbitals of Pt. The potential energy surface in figure 2.9(b) is for both Pt(111) surface and the W tip. Thus, potential energy surface for bare Pt(111) sample is strongly modified by a W tip approaching to physisorbed Xe atom. The tip height h_t here is $6.0\mathring{A}$. The minimum of the potential energy is displaced by the moving tip.

To find the positions of the local minima contours of the potential energy surfaces are calculated for two different tip heights, $h_t = 6.00\mathring{A}$ and $h_t = 4.00\mathring{A}$. In figure 2.10(a) and 2.10(b), these contours are shown. The possible Xe positions are labeled by "x". The positions for the local energy minima corresponding to larger tip-surface separation lie on the tip site. In this case, the atoms at the second layer of the tip determines the possible binding sites. For lower tip heights, like $h_t = 4.00\mathring{A}$ in figure 2.10(b) the positions of the local minima are changed and became farther from the tip apex.

2.2.3 Controlled Lateral Translation: Dynamics

The lateral motion of Xe on the Pt(111) surface is investigated by performing molecular dynamics calculations. The tip is moved along the major symmetry directions of the surface. The set of coordinates of Xe and the tip are labeled by (ξ, κ, ζ) and (x, y, z) respectively. The time step is $\delta t = 1.0 \times 10^{-14} s$ and the tip is moved with a constant speed $v_t = 4.801 \times 10^{10} \mathring{A}/s$ in the $[\bar{1}\bar{1}2]$ direction and $v_t = 5.544 \times 10^{10} \mathring{A}/s$ in the [110] direction. The results of calculations for the motion of the tip along the κ direction with different heights are summarized in

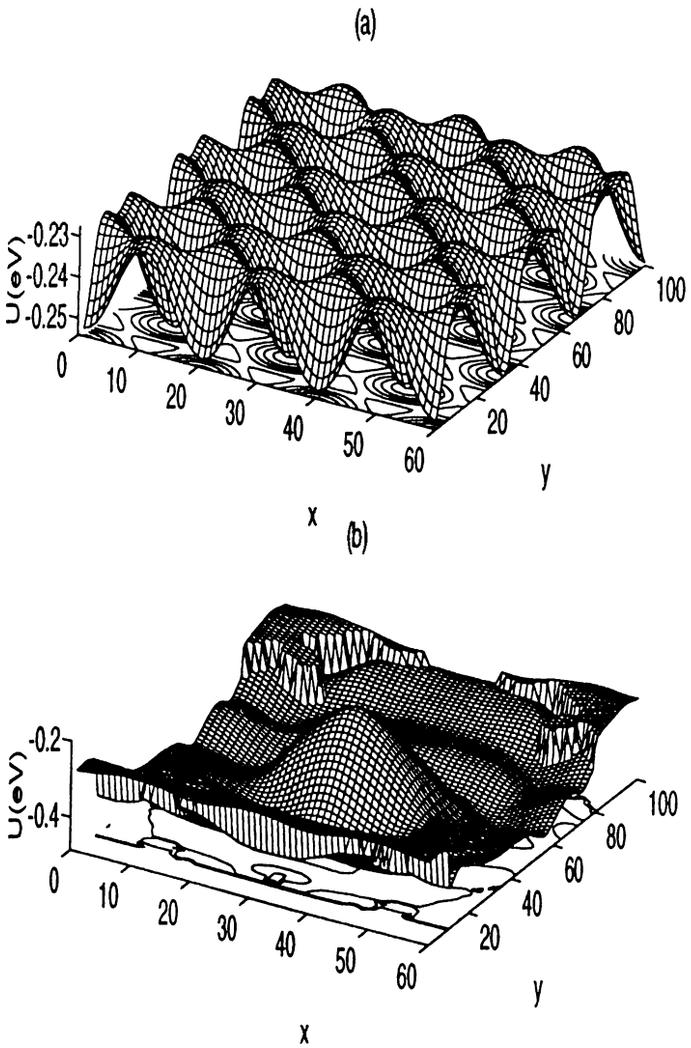

Figure 2.8: Potential energy surfaces
(a) The potential energy of Xe on the Pt(111) surface. (b) The total potential energy of Xe on the Pt(111) surface with a W(111) tip lying 6.0$\AA$ above the surface. These plots cover (3×3) unit cells of the Pt(111) surface.

figure 2.11. The tip moves from a distance towards Xe in different heights. Figure 2.11(a) illustrates the motion of Xe in $[\bar{1}\bar{1}2]$ direction (κ) induced by the motion of the tip in the same direction (y). For $h_t = 8.00\AA$, the Xe atom is practically unaffected, but when the height is decreased to $7.50\AA$, the Xe is attracted by

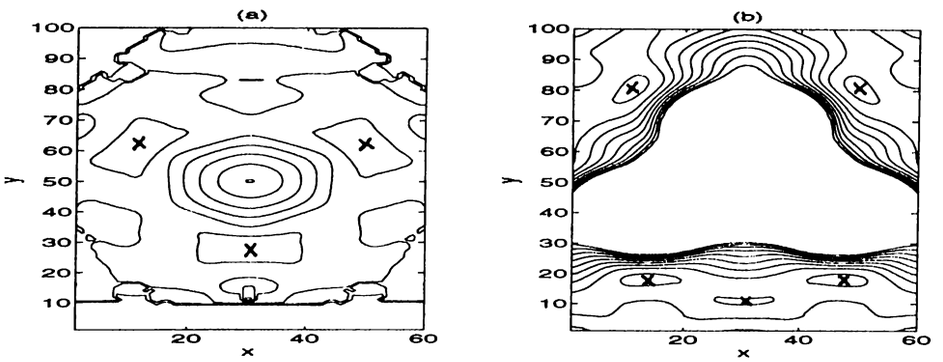

Figure 2.9: Contours of the potential energy surfaces
Contours of the potential energy surfaces for tip heights (a) $h_t = 6.00\mathring{A}$ and (b) $h_t = 4.00\mathring{A}$.The possible Xe positions are labeled by "x".

the tip. In this range of h_t, the atom moves rather freely in a large volume. For $7.00\mathring{A} \leq h_t < 5.00\mathring{A}$, the Xe is attached to the tip and carried out without showing any periodicity due to surface corrugation. However, upon the decrease of h_t i.e, $5.00 \leq h_t$, the atom begins to feel surface corrugation and perform a periodic motion, showing the surface periodicity in $[\bar{1}\bar{1}2]$ direction. Figure 2.10(b) is the real space trajectory of Xe in $\kappa - \xi$ plane. For $5.00 \leq h_t$, the atom escapes sideways initially to a surface minimum. In the course of carriage, the atom shows small deviations in the [110] direction. Molecular Dynamics calculations are performed for motion in the [110] direction with the tip geometry which is used for the motion in the $[\bar{1}\bar{1}2]$ direction (triangle, pointing the positive y direction) and turning the tip ninety degrees (triangle, pointing the positive x direction) also. The behaviour of the motion is similar to that described in figure 2.10, despite minor changes. One can easily see that, while Xe performs periodic motion for $h_t = 4.00\mathring{A}$, it passes some portion of each period quickly and passes other portion much slower. This is very similar to the "Stick-Slip" phenomena, observed in AFM experiments.[48] The sample force acting on the Xe atom, which is shown in figure 2.11, is also very similar to the force measured on the tip in AFM experiments. The sample forces on Xe in previous section had different character.

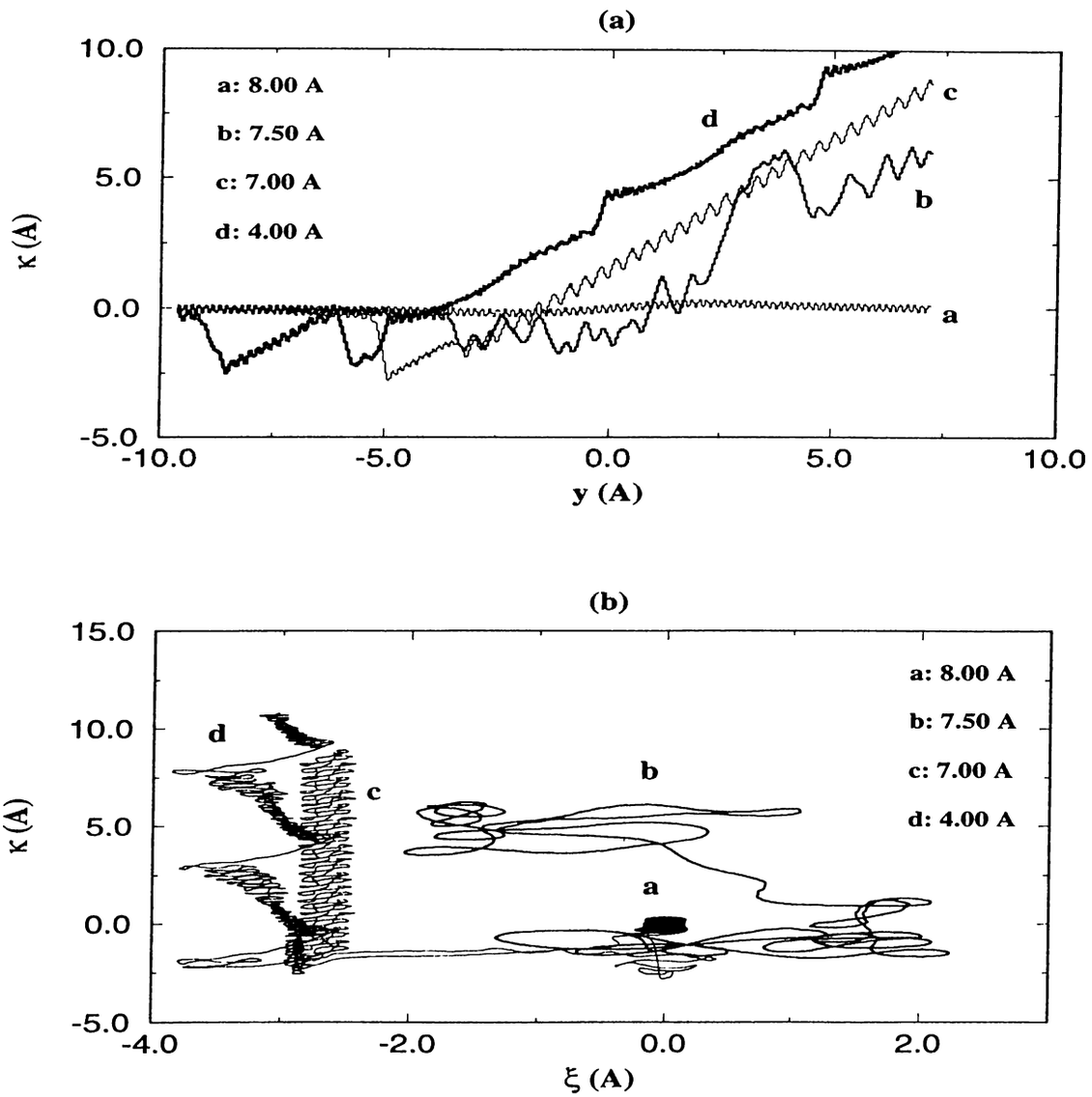

Figure 2.10: Lateral translation of Xe on the Pt(111) surface
Lateral translation of Xe atom induced by the tip along the $[\bar{1}\bar{1}2]$ direction with different tip heights above the Pt(111) surface. (a) Motion of Xe vs. motion of the tip. y and κ are the coordinates of the tip and Xe along the $[\bar{1}\bar{1}2]$ direction, respectively. (b) Trajectory of Xe during the motion on $\kappa - \xi$ plane.

In order to obtain a general understanding about the motion of the Xe atom on metal surfaces, the motion of Xe on the Pt(111) surface is compared with the motion of Xe on the Ni(110) surface. There are many points of view to

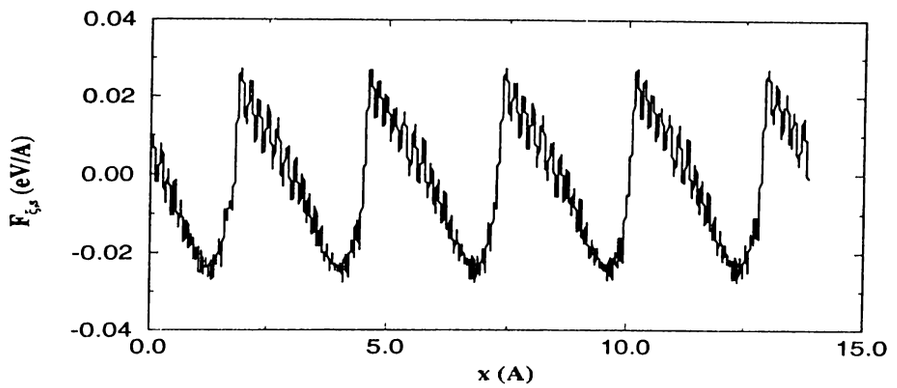

Figure 2.11: The force due to sample on the Xe atom
The force on the Xe atom due to the sample is shown for the Xe motion induced by the tip motion along the [110] direction. ($h_t = 4.00\mathring{A}$.)

compare these two motions but, we deal with the energetics first then compare the results of the method of molecular dynamics. The binding energy of Xe on the Ni(110) surface does not differ so much from the binding energy of Xe on the Pt(111) surface although the adsorption sites are different. This is not the case when the energy barriers for lateral motion are compared. The energy barriers on the Ni(110) surface are much more higher then the barriers on the Pt(111) surface. The relative differences between the energy barriers belonging to different directions are also important, since the atom may choose the direction of the lower barrier. There is an important difference between the barriers for the motion along the $[1\bar{1}0]$ direction and the [100] direction, on the Ni(110) surface. Such kind of relative difference of the barriers is not seen on the Pt(111) surface. Generally the results of the molecular dynamics simulations are consistent with energy differences discussed above. The threshold heights of the motion of the Xe atom on the Pt(111) surface are higher then the threshold heights of the motion on the Ni(110) surface. As there is no important relative difference between the barriers, the threshold heights of the motion along the [110] direction and the $[\bar{1}\bar{1}2]$ direction on the Pt(111) surface are the same. The Xe atom moves more freely on the Pt(111) surface. The paths of Xe on the Ni(110) surface are more regular showing the surface periodicity. Another consequence of the surface

corrugation is that, there are more modes of motion on the Ni(110) surface. Tip corrugation determines the motion on the Pt(111) surface for high h_t values. If a sample surface is completely flat then the atom will always move with the tip minima move. The atom is pushed along the $[1\bar{1}0]$ direction but not in the [100] direction on the Ni(110) surface. One reason for this can be the magnitude of the surface barrier but another reason can be the slope of the surface potential energy. Surface corrugation, the magnitude, the relative differences and slopes of the barriers determine the modes of the motion.

The equilibrium site of the Xe atom on the Pt(111) surface is top site. It is achieved by the term which is used to describe the interaction with the delocalized conduction electrons. The reason of having lower energy barriers on the Pt(111) surface can be this interaction also. Another important point to consider is the effect of relaxation. Some of the tip and the sample were not kept at their ideal positions and were able to move. Their motions have modified the barriers and affect the translation of the Xe atom. A brief conclusion including remarks on the lateral translation of Xe at the last chapter.

Chapter 3

CONTROLLED PERPENDICULAR MOTION OF Xe

The idea that an atom could be transferred between tip and sample surface is due to Gomer. His idea has been subject of both experimental and theoretical studies. Lyo and Avouris removed and redeposited individual Si atoms from Si(111) surface by reducing the tip-sample distance. Mamin, Guethner and Rugar demonstrated that with a low threshold field, gold atoms were emitted from the gold tip to the gold substrate in a controlled and reproducible way. Based on the self-consistent pseudopotential calculations for an Al adatom between the two Al(100) electrodes Ciraci et al. discussed the conditions for the atom transfer extensively. Lang studied the field-induced transfer of an Al and Si atom by using atom-on-jellium model[49,50] The most important and well known experiment has been the Atom Switch, realized by Eigler, Lutz and Rudge. They transferred Xe atom from the Ni(110) surface to a W tip reversibly, in a controlled manner. Their work has attracted much interest because it led to the smallest atomic-scale electronic device with bistable conductance. Important features of the Atom Switch can be summarized as follows:

- Xe is always transfered towards the positively biased electrode.
- At small tip-sample distance (corresponding to resistance $R < 700K\Omega$) the Xe atom moves spontaneously to the tip without applying a positive voltage pulse. At larger separation ($R > 1.5M\Omega$) however, Xe either hops on the Ni surface or escapes from the junction region entirely. (There is platue at $5.7K\Omega$ which correspond to a point of contact.)
- Depending upon the location of xenon at kink sites, on the bare Ni(110) terrace, on top of a single Ni adatom on the Ni(110) surface the conductance ratio range from unity to 7.
- There is characteristic transfer rate for a fixed tip-sample distance. According to Eigler et al, for a $906K\Omega$ junction, the transfer rate exhibits a power-law dependence on the pulse voltage and consequently on the tunnel current I. They propose the relation $\tau^{-1} \propto I^{4.9\mp0.2}$.

Earlier mechanisms responsible for the atom transfer and hence physics of this atomic scale, bistable electronic switch have been investigated by various authors. In spite of several theoretical studies, the Atom Switch is not fully understood yet. Eigler et al. proposed heating assisted electromigration as the mechanism responsible for the atom transfer, but several different mechanisms were proposed thereafter. Walkup, Newns and Avouris examined different mechanisms[51] and concluded that multiple vibrational excitations of an adsorbate via inelastic electron tunneling plays an important role in the transfer of the Xe atom. Later, Salam et al.[52] examined atom transfer and proposed that inelastic tunneling of a single electron induces coherent multiple excitation of the adsorbate-substrate bond. They found this mechanism is favorable for systems, such as Na adsorption on Cu or O_2 adsorption on Pt. Brandbyge and Hedegard considered the Xe atom as a quantum Brownian particle in nonequilibrium environments.[53] Sáenz and Garcia found that the atom transfer could be understood in terms of a thermally assisted single atom tunneling process,[54] but not in terms of a heating assisted electromigration as proposed by Eigler et al. Using the fact that charge

is transferred from metal to the 6s resonance of the Xe atom, Sáenz and Garcia were able to reproduce the observed dependence of the transfer rate on the voltage pulse at high V region only for very large (but unusual) effective charge of Xe atom ($q_{eff} = 0.3e$). None of these works are conclusive about the atom transfer.

A precise description of the mechanism shall involve detailed account of the interaction between the surface and Xe, as well as the weak ionic bond constructed therefrom. These are not fully described by empirical potential used in the previous theoretical calculations. Also the variation of the charge on the Xe atom and of the induced dipole moment with the distance between the Xe atom and the electrodes has to be considered. In previous studies, the charge on the Xe atom was assumed to be constant. It was even totally neglected in some calculations. In this thesis work, by using simple models, we analyze various features of the substrate-Xe interaction which are relevant for various mechanisms responsible for the atom transfer. We then investigate the contribution of these mechanisms in the observed rate of the atom transfer. For lack of first principle and self-consistent treatments for detailed description of the bond together with short and long range interaction, we used an empirical potential. Such a method is affordable, and sufficient for the correct description of the atom transfer with reasonable accuracy.

In this chapter, the potential energy of Xe between two flat Pt(111) electrodes is generated from the empirical potential given by Barker and Rettner. The form of potential energy curve, especially the barrier between two wells at each sample site vary with the distance between two surfaces. In particular, under an applied voltage the symmetry of the curve is destroyed and the barrier is reduced if Xe is charged. To this end, by using Anderson-Newns theory the effective charge of Xe is calculated as a function of Xe-surface distance. The quantum states of Xe between two electrodes under a bias voltage and thermally assisted (tunneling and ballistic) transmission to the adjoint well are calculated to obtain the transfer rate of Xe. The contribution of dipole excitation and resonance mechanisms to the transfer rate are also calculated.

3.1 POTENTIAL ENERGY OF Xe

The controlled motion of Xe atom in the ζ direction ([111] direction for Pt(111) surface) is studied between two flat Pt(111) surfaces. Barker and Rettner were able to determine an accurate empirical potential energy function for the interaction of Xe with the Pt(111) surface, which is consistent with a wide range of dynamical and equilibrium experimental data. This potential leads to an equilibrium position of a single Xe atom directly above a surface platinum atom (top-site). We generate the potential energy of Xe between two flat Pt electrodes by using the empirical potential considered in the lateral motion, in chapter 2. In the present case, the W tip is replaced by a flat Pt(111) surface as the second electrode. This way , several unknown factors related to the tip structure are eliminated. Normally, the potential energy of Xe between two electrodes is expected to yield two wells separated by a barrier which changes into a single well at small separation. Using directly the Barker and Rettner's empirical potential, we obtained not two but three wells for relatively smaller separations. The third shallow well occurs at the center. This is perhaps due to the limitation of the interpolation between the short range part and the long range part of the potential function. If this were the real situation, the resonant tunneling of atoms would occur across the wells in appropriate conditions. The Eigler experiment does not give evidence for the resonant tunneling of atoms. Hence, three well structure is probably an artifact. The connection (interpolation) between two ranges of the empirical potential is improved to lead to usual double well structure for small s. In figure 3.1(a) the potential energy curves $V(\zeta, s)$ associated with the xenon atom between two flat Pt(111) surfaces are shown along the [111] direction for different electrode separations, s. For certain range of s, the $V(\zeta, s)$ curve has a double well structure separated by an energy barrier $Q(s)$, and it is symmetric at zero bias due to the symmetry of the electrodes. However, it is asymmetric for finite bias voltage or usual tip-sample system. In figure 3.1(b), the variation of potential barrier $Q(s)$ with s is illustrated. By reducing the separation between the electrodes, the potential barrier $Q(s)$ decreases, and eventually the double

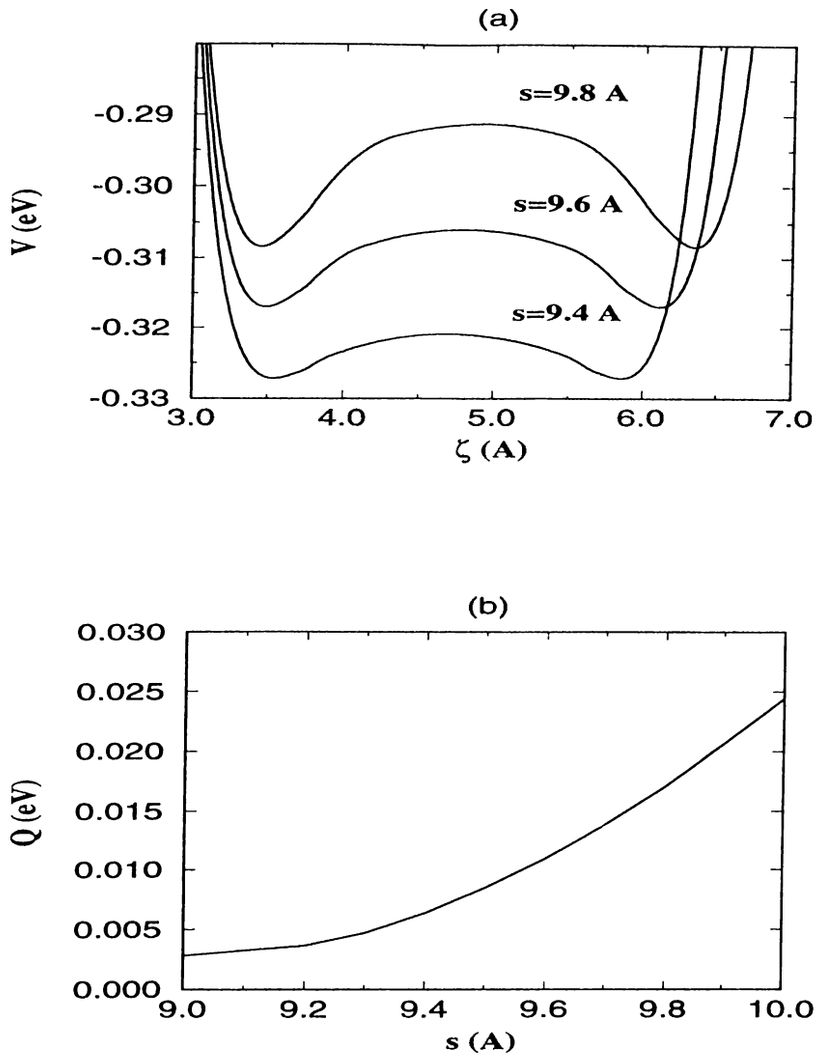

Figure 3.1: Potential energy curves and energy barrier
(a) Variation of the potential energy of Xe, $V(\zeta, s)$ with s along the [111] direction; Xe is between two top sites of Pt(111) electrodes. (b) Variation of the barrier energy $Q(s)$ with the separation of electrodes

well structure disappears forming a single well.

The quantum states of the Xe atom for the above potential energy can be determined from the solution of the Schroedinger equation for 3D potential energy formed by all the tip and the sample atoms. Owing to the symmetry in the $[\bar{1}\bar{1}2]$ and [110] direction, it is sufficient, however, to consider the variation of

the potential energy only in the [111] direction. Eigenvalues and eigenstates of $V(\zeta, s)$ are found by solving the time independent, 1D Schroedinger equation. The Xe atom is assumed to be initially in the states which are located at the sample site indicating the fact that it is observed on the sample surface.

Normally, the atom can transfer to the other side only by tunneling even in the absence of the applied voltage. The tunneling probability is nevertheless negligible. Upon the decrease of the separation, and hence the decrease of the potential barrier, the tunneling probability of the Xe atom to the other side increases. Sáenz and Garcia[54] found that there is a nonzero probability of atom transfer even at zero voltage and calculated the transfer rate due to tunneling. The same method is used for the calculation of the transfer rate assuming thermally assisted tunneling. The transfer rate τ^{-1} is expressed as

$$\tau^{-1} \approx \frac{\sum_i \omega_i e^{E_i/k_B T} T(E_i) \delta(E_f - E_i)}{\sum_i e^{E_i/k_B T}} \tag{3.1}$$

where ω_i is the frequency and E_i is the eigenvalue of the i^{th} state on the sample side. $T(E_i)$ is the tunneling probability which is calculated within the Wentzel-Kramers-Brillouin-Jeffreys (WKBJ) approximation, since the atom wavelength is much smaller than the width of the barrier. E_f is the eigenvalue of the final state which must be equal to E_i. The tunneling probabilities are very small for the low energy states, but become considerable for the states close to the top of the potential barrier. The calculated transfer rates are shown in figure 3.2 as a function of the tip-sample separation s. The rate is small for large separations, but for $s \leq 9.5\mathring{A}$ one transfer may occur in each second. Note that in the Eigler's experiment, the Xe atom moved spontaneously to the tip without applying a positive voltage pulse for small s. This separation s can be $s \sim 9.5\mathring{A}$ for the transfer of Xe between two Pt(111) electrodes, in the present case the zig-zags in the $\tau^{-1}(s)$ curve arises because of finite number of states n_{ws} in the sample-site well. While Q varries smoothly with s, the variation of n_{ws} and transmission occuring thereof are discontinuous. This quantum size effect will be discussed later.

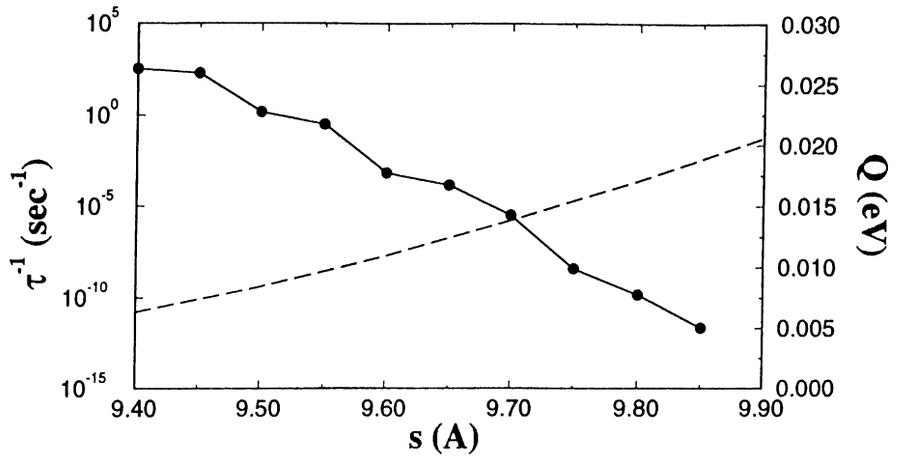

Figure 3.2: The transfer rate for the tunneling of the Xe atom
The transfer rate for the tunneling of the Xe atom and potential barrier Q versus the tip-sample separation s

3.2 Xe TRANSFER WITH BIAS VOLTAGE

Owing to the symmetry of the electrodes the calculated potential energy curves $V(\zeta, s)$ are symmetric with respect to the center of the barrier, and $Q_+ = Q_-$ (Q_+ or Q_- being barriers for two different directions). This symmetry can be removed by an external agent such as applied bias voltage. If the net charge on the Xe atom is not zero, there will be an electrical force on the atom when a bias voltage is applied to one of the electrodes. Upon the application of bias voltage; one barrier increases while the other barrier decreases. This, directly affects the transfer rate.

3.2.1 Effective charge on the Xe atom

The effective charge q_{eff} on the Xe atom is crucial for the modification of the $V(\zeta, s)$ and hence the transfer rate. Based on the calculation of the atom-on-jellium model, Eigler et al. have found that the Xe $6s$ resonance has non-zero local state density at the Fermi level. The visibility of adsorbed Xe in STM[22] has been attributed to the partial filling of the 6s resonance state. This occurs inspite of the fact that 6s state of the free Xe atom lies 3-4 eV above the Fermi

level. Arguments for the partial filling of the Xe-6s state follows. Wandelt and Gumhalter presented a model called "s-resonance model" which incorporates Van der Waals and charge transfer effects due to partial filling of the 6s resonance.[55] They found direct support from the UPS of the valence band and Xe $5p_{3/2,1/2}$ state of the xenon covered Pd surfaces. SCF pseudopotential calculations within the LDA have provided strong evidence that there is significant chemical interaction. Hence, it has been shown that the charge transfer from metal surface to Xe is crucial in the bonding. Empirical LCAO calculations by Perez et al.[47] confirmed these results and found excess charge of $q_{eff} \cong 0.1$ electrons. It is now commonly accepted that adsorbed xenon is negatively charged. Second question one has to answer is the variation of the charge with separation. Sáenz and Garcia assumed that the effective charge on the Xe atom was constant and equal to $0.1|e|$. As ponited out earlier in this thesis, the 6s state of a free Xe atom is normally empty, but upon physisorption, the 6s state becomes a resonance and partially filled. It is expected that the charge (or occupation) of the 6s state changes with separation. The magnitude and variation of this charge are still controversial.

Duc to Newns-Anderson model, the resonance of a chemisorbed atom on a metal surface is a Lorentzian function with a single peak of width $\sim 2\Delta$, centered at the energy $\epsilon = \epsilon_a + \Lambda$ when the energy dependence of Δ and Λ is neglected. (see chapter 1, equation 1.14) Newns proposed a model for the chemisorption of H on 3d transition matels. He assumed that the dominant coupling constants V_{ak} are the ones which connect the $|1s\rangle$ to states $|k\rangle$ in the metal d-band. The d-band states $|k\rangle$ can be written as a generalization of the tight-binding form for Bloch states.

$$|k\rangle = \sum_i \sum_{\alpha=1}^{5} |i,\alpha\rangle\langle i,\alpha|k\rangle \tag{3.2}$$

i denotes the surface atoms and α denotes the orbitals of the atom i. Substituting this equation into the equation 1.15

$$\Delta(\epsilon_a) = \pi \sum_{i,\alpha} \sum_{j,\beta} \langle a|V|i\alpha\rangle\langle j\beta|V|a\rangle \sum_k \langle i\alpha|k\rangle\langle k|j\beta\rangle \delta(\epsilon - \epsilon_k) \tag{3.3}$$

In view of the quasi local character of the metal d-states, the matrix elements $\langle a|V|i\alpha\rangle$ connecting the adatom orbital to the neighboring metal d orbitals $|i,\alpha\rangle$

dominate the the above summation. Therefore, we consider a simple model which considers the bonding of Xe to the Pt(111) surface locally. Furthermore, we assume that the main contribution to the Δ comes from the nearest Pt atom's $|\psi_{6s}\rangle$ and $|\psi_{5d}\rangle$ orbitals. The electronic configurations of free Xe and Pt atoms are

Xe : $/5p^6 6s^0$

Pt : $/5d^9 6s^1$

If the Xe atom and the nearest Pt atom are considered on the z-axis, then the Xe-6s orbital is confined to the Pt-5d orbital which has Y_{20} as the angular part. Then Δ can be expressed as

$$\Delta \simeq \pi c_0 |\langle Xe-6s|V|Pt-6s\rangle|^2 + \pi c_1 |\langle Xe-6s|V|Pt-5d_{20}\rangle|^2 \qquad (3.4)$$

$\langle Xe-6s|V|Pt-6s\rangle$ and $\langle Xe-6s|V|Pt-5d_{20}\rangle$ are the matrix elements and they can be approximated as

$$\langle Xe-6s|V|Pt-6s\rangle \propto \langle Xe-6s|Pt-6s\rangle \cdot \frac{\epsilon_{Xe-6s}+\epsilon_{Pt-6s}}{2} \qquad (3.5)$$

$$\langle Xe-6s|V|Pt-5d_{20}\rangle \propto \langle Xe-6s|Pt-5d_{20}\rangle \cdot \frac{\epsilon_{Xe-6s}+\epsilon_{Pt-5d}}{2} \qquad (3.6)$$

ϵ_{Xe-6s}, ϵ_{Pt-6s} and ϵ_{Pt-6s} are the energy levels of free Xe and Pt atoms. The overlap integrals $\langle Xe-6s|Pt-6s\rangle$ and $\langle Xe-6s|Pt-5d_{20}\rangle$ (denoted by S_1 and S_2 respectively), are calculated numerically by using Herman-Skillman atomic wavefunctions. Solving the non-relativistic Hartree-Fock-Slater equations self-consistently, Herman and Skillman developed a numerical method[56] to obtain radial wavefunctions of all the atoms within the Local Density Approximation. (LDA) At the equilibrium distance between the Xe atom and the Pt(111) surface, the values of S_1 and S_2 are calculated 0.44 and 0.0045. respectively. Consequently, the second term in equation 3.4 is negligible. Then, c_0 is taken to be unity, and Δ is calculated as $\sim$ 1.02 eV. This model gives that the electron at the Pt-6s state fills partially the Xe-6s resonance. The position of the Xe-6s resonance is determined by using the spin-polarized photoelectron spectroscopy.[57] The Xe-6s resonance lies 3.91 eV above the Fermi level. Integrating the part of this

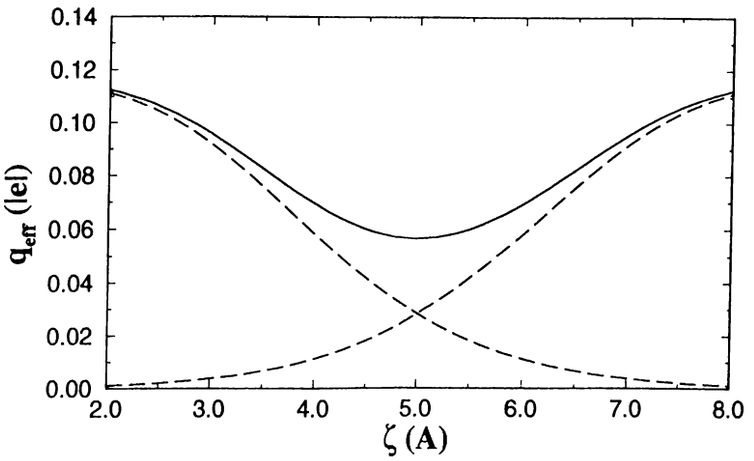

Figure 3.3: Charge on the Xe atom
The variation of the charge q_{eff} with ζ. Xe adsorbed on the Pt(111) surface or tip (dashed lines) and Xe between two Pt(111) surfaces. (solid line)

resonance dipped in the Fermi level yields the occupation number n.

$$n = \frac{1}{2} - \pi^{-1} \arctan(\frac{\bar{\epsilon}_{Xe-6s}}{\Delta}) \tag{3.7}$$

$\bar{\epsilon}_{Xe-6s}$ is the position of the Xe-6s resonance with respect to the Fermi level. ($\epsilon_F = -5.65eV$) The occupation number n is found to be $\sim$ 0.081 for the equilibrium Xe-Pt(111) distance. Figure 3.3 shows the effective charge of the Xe atom as a function of ζ (the separation between Xe and the Pt(111) surface). Dashed lines correspond to the charge when only sample or tip is present. These right and left curves are added to give the charge in the presence of sample and tip. The additivity of the effective charges associated with each electrode is a good approximation for relatively large s. When a positive bias is applied to the other electrode, an electrical force will act on the Xe atom due to this charge. The potential energy term due to the bias voltage can be written as

$$\Delta U(\zeta) \simeq -q_{eff} V \frac{\zeta - d_{im}}{s - 2d_{im}} \tag{3.8}$$

Here, q_{eff} is the charge on Xe which is assumed to be equal to the charge due to the 6s resonance; d_{im} is the image plane position from the atomic Pt(111) plane. Using the method described in reference 55, d_{im} is calculated to be $\simeq 2.04\mathring{A}$.

$\Delta U(\zeta)$ decreases linearly and reduces the barrier only when the charge q_{eff} is constant. However, the variation of the barrier with ζ is not obvious if the value of q_{eff} varies with ζ. If q_{eff} is assumed to decrease exponentially, in the form $\sim e^{-\beta\zeta}$ for a single electrode, the barrier increases for $\beta > 0.88$ but decreases for $\beta \leq 0.88$ for $s = 10.0\mathring{A}$. In figure 3.4(a), the variation of potential energy $V(\zeta, s)$ of xenon between two Pt(111) electrodes is illustrated for different bias voltages. The barrier to the transfer of Xe from the sample to the tip is reduced for higher voltages. In figure 3.4(b), the barrier Q vs. bias voltage V_B is shown for different tip-sample separations. Note the dependence of $Q(V_B)$ on the variation of q_{eff} with distance. The barrier lowering with V_B becomes dramatic when q_{eff} is constant. In view of this result, earlier studies which used constant q_{eff} are seriously questioned.

3.2.2 Transfer Rates for the Asymmetric Potential

The calculation of the transfer rate due to tunneling without bias voltage was described before. If a bias voltage is applied to one of the electrodes, our potential becomes asymmetric and the eigenvalues and the eigenstates of the Xe atom are changed. Initially the Xe atom is taken to be in the state localized on the sample side, but it can be also at the states above the barrier after the onset of the voltage pulse. The thermal probability of the Xe atom to be at the i^{th} state is

$$P_T^i = \frac{e^{E_i/k_BT}}{\sum_j e^{E_j/k_BT}} \tag{3.9}$$

In the case of the asymmetric potential, the lowest energy state of the tip side is lower then the lowest energy state of the sample side. Thus, a state above the barrier is less probable with respect to the tip side due to equation 3.9 . If the energy of the i^{th} state lies below the barrier, the atom tunnels to the other side. Then the rate of tunneling is obtained by summing the tunneling probabilities from the states localized at the sample side. That is

$$\tau_T^{-1} = \sum_i P_T^i \cdot \omega_i \cdot T(E_i) \cdot \delta(E_f - E_i) \tag{3.10}$$

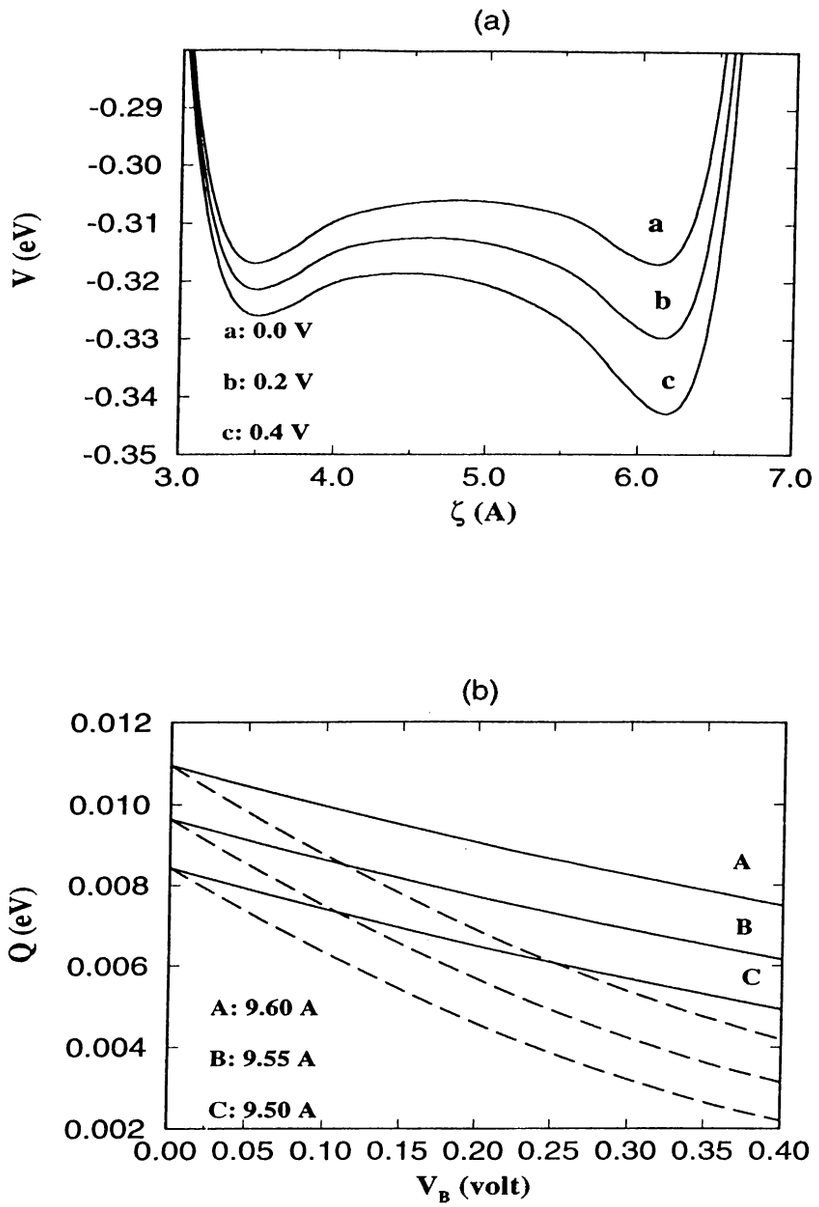

Figure 3.4: Potential energy curves for different bias voltages
(a) The potential energy curves $V(\zeta, s)$ of xenon between two Pt(111) electrodes for different bias voltages. (b) The potential barrier Q for Xe transfer from the sample to the tip as a function of applied voltage. The dashed lines are the Q values corresponding to the $q_{eff} = 0.1|e|$ and constant throughout the barrier.

This expression is only for the energy levels below the top of the barrier. Above

the potential barrier, the atom normally oscillates in the well upon interaction with the tip. It loses energy in a dissipative medium. Consequently, it decays to the lower energy states. For the states above the barrier, the atom is in thermal equilibrium state at the sample side but at non-equilibrium at the tip side. In calculating the contribution of the states above the barrier, the thermal probability at the tip side must also be considered. We now discuss the energy dissipation of the transferred Xe at the tip site.

There are two mechanisms for the relaxation of the Xe-surface vibration (or dissipation of energy of Xe upon interaction with the surface): i) Electron-hole pair mechanism ii) Energy transfer to the metal phonons. Persson calculated the energy relaxation time due to excitation of the $e-h$ pairs for Xe on the Ag surface[58] and found $T_{e-h} \sim 3 \times 10^{-9}$ s. In a different study, Gao et al.[59] found almost the same value for Xe on Ni. Damping by phonon mechanism is much efficient. In the elastic continuum model,[60,61] Walkup et al.[51] calculated the vibrational lifetime for the first excited state of a xenon on the Ni surface and found that $t_P \simeq 25$ ps. For the higher vibrational levels, they took the relaxation rates γ $(= t_P^{-1})$ of a harmonic oscillator. That is $\gamma = n.(t_P^{-1})$ for the n^{th} excited state. In the elastic continuum model, the vibration frequency ω is assumed to derive waves in the elastic medium of the substrate with the same frequency. These waves damp the vibration by radiating energy away from the region. Using this model, the vibrational lifetime for the first excited state of Xe on the Pt(111) surface is found to be $t_P \simeq 20$ ps for $s = 9.6\mathring{A}$ and $V_B = 0.100$ V. The lifetimes of the higher lying levels fall quickly. For example, the lifetime of an excited state few quantum numbers higher than the ground state becomes less than one period of Xe. We assume that the Xe atom is losing its energy after one "collision" with the tip so we take the lifetime as one period of the oscillation of Xe. The transfer rate for the levels above the barrier is calculated by

$$\tau_B^{-1} \simeq \sum_j (P_{TS}^j - P_{TT}^j) \cdot \omega_j \tag{3.11}$$

P_{TS}^j is the thermal probability of the level j relative to the sample side lowest level and P_{TT}^j is the thermal probability relative to the tip side lowest level. If

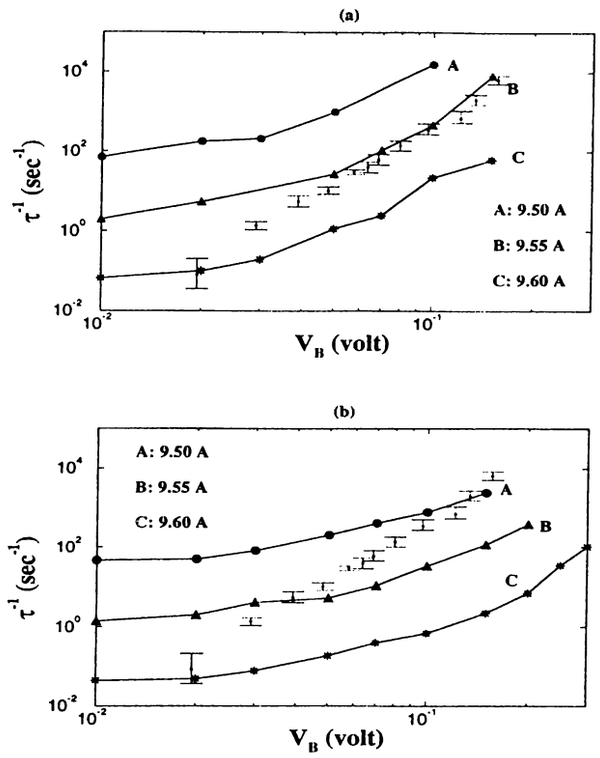

Figure 3.5: The transfer rates due to tunneling and thermal probabilities as a function of applied voltage

The transfer rates due to tunneling and thermal probabilities as a function of applied voltage V_B for tip-sample separations A: 9.50$\AA$, B: 9.55$\AA$ and C: 9.60$\AA$. (a) The charge of Xe is kept fixed at $q_{eff} = 0.1|e|$, and (b) the charge varies with the position of Xe. Experimental data correspond to the Ni(110) surface and the W-tip are also shown by bars for the sake of comparison.

these probabilities are equal like in the symmetric potential case, the net transfer rate due to this level is zero. In this case, the atom is at thermal equilibrium. The calculated transfer rates are shown in figure 3.5(a) as a function of applied voltage for three different tip-sample separations and for constant effective charge ($q_{eff} = 0.1|e|$) on Xe. These transfer rates include contributions from states below and as well as above the barrier. ($\tau^{-1} = \tau_T^{-1} + \tau_B^{-1}$) In figure 3.5(b) the calculated transfer with the variable effective charge is illustrated. For the sake of comparison, the data obtained by Eigler et al.[21] for Xe-Ni(110) surface are shown in the same figures. Two important points are worth discussing. First, the

calculated transfer rates do not exhibit a power law dependence and they have nonzero values for zero bias voltage. Second, the variation of transfer rates with the bias voltage and especially with the separation s is not smooth. The reason is that there are small numbers of discrete levels responsible for the transfer. This discrete nature can be regarded as a quantum size effect where the discrete energy levels affect the transfer rates. The last levels below the potential barrier and the first levels above the barrier yield dominant contributions to the transfer rates. Barrier lowering changes the positions of energy levels and hence leads to discontinuous changes in the spectrum relative to the barrier. This gives rise to sudden changes in the transfer rate. Having examined the tunneling and ballistic process under the applied bias voltage, we now take a look for other possible mechanisms.

3.3 Other Mechanisms

3.3.1 Electromigration

We can think about other physical mechanisms which can either contribute to or become responsible for the transfer of the Xe atom. One mechanism is the heating assisted electromigration.[62,63] The term electromigration is used for the net motion of atomic defects within a material that results when a current is passed through the sample. The forces in electromigration is divided into two components. i) The direct force due to bulk electric field acting on the defect. ii) the "electron-wind force" due to momentum transfer from the electrons to the defect. There are two main approaches for electromigration. One is the Fiks-Huntington ballistic model of electromigration[64,65] in which one assumes both a free-electron-gas model and that all of the momentum lost by scattered electrons is transferred to the defect. Second approach is due to Bosvieux and Friedel[66] that go beyond the free electron model. As the defect scatters the conduction electrons, an applied current induces a charge polarization about the defect. Ralls, Ralph and Buhrman have studied the electromigration in

metal nanobridges[62] and developed a model of electron heating of the defects. They first calculate a characteristic "temperature" of the nonequilibrium electron distribution as a function of sample bias. Then they estimate the actual defect temperature T_d by finding the steady-state temperature when it is coupled to the electrons at temperature T_{el} and the lattice at temperature T_l. They give T_{el} as

$$T_{el} = (T_{el,max} - T_l)/\Theta + T_l \tag{3.12}$$

where $T_{el,max}$ is the maximum effective electron temperature that is found at the center of the nanobridge; Θ is the scaling parameter for a location other than the center. The defect is not at the electron temperature but it loses its energy to the lattice and lies at temperature between T_{el} and T_l. Finally, they propose a function for the defect temperature in the form

$$T_d = \frac{T_{el}}{\alpha} + T_l(1 - 1/\alpha)\frac{T_l}{T\epsilon l} \tag{3.13}$$

Here, α is defined as $(\gamma_{el} + \gamma_{ph})/\gamma_{el}$ where γ_{el} and γ_{ph} are the relaxation rates due to electrons and phonons, respectively. They used s and α as fitting parameters and fit the measured defect temperature data.

Turning back to the transfered Xe atom, one can see a good resemblance between these two phenomena. The Xe atom can be heated up by the conduction electrons. Sáenz and Garcia assumed that the heating of the Xe atom occurs in the same manner outlined above. They approximated the atom temperature as $T_a \approx T + C \times V^2$ due to the Ralls et al.'s experimental data. They concluded that for any C value, the transfer rate due to T_a differs from the Eigler's experiment so heating assisted electromigration can not be the mechanism for the transfer of Xe atom. Walkup et al.[51] presented a simplified picture. The average momentum change per electron Δp would be related to the average energy transfer ΔE, by $\Delta E \sim (\Delta p)^2/2M$, where M is the mass of Xe. Momentum transfer results in an "electron-wind force" $F_w \simeq (I/e)\Delta p$. They concluded that the contribution of the wind force is negligible. For a better understanding of the contribution of electromigration, one has to find the electron temperature T_{el} and relaxation rates γ_{el}. Then, by using equation 3.12 the effective atom temperature can be found.

3.3.2 Inelastic Electron Tunneling

Since electrons are tunneling between two electrodes, they can heat the sample and the tip or induce vibrational excitations by inelastic tunneling. A hot electron in a metal will decelerate by emission of phonons or by excitation of electron-hole pairs. With typical values of tunnel current, voltage, and heat conductivity, the temperature rise in metals can be $\Delta T \approx 10^{-4} K$ which is negligible. However, the localization of a substantial energy in a bond, like a bond between an adatom and surface, by the way of inelastic tunneling may cause vibrational excitations.[67] There are two processes relevant for the inelastic electron tunneling between a metal tip and a metal surface with a chemisorbed atom or a molecule: i) Dipole excitation[67] ii) Resonant tunneling.[68] In the first process, a tunneling electron interacts with the transition dipole moment of the adatom-surface vibration. In the second process the tip is centered above the atom and a potential V is applied so there will be an effective channel via a resonance of the atom. Then, an electron which is tunneling will be trapped temporarly in this resonance. The additional charging of the adatom will lead to a change of the internuclear potential. As soon as the electron hops from the resonance to the conduction band of the substrate, the atom can be left in a vibrational excited state. Later, the excitation (or stored) energy is dissipated through the lattice. The dissipation of energy in the inelastic electron tunneling process through these two processes is conveniently treated in terms of the conductance. In what follows we take a close look at these two processes, and find out their contribution to the transfer of Xe.

The net change σ_{dip} in the normalized conductance (the ratio of inelastic tunneling conductance to total conductance) due to dipole mechanism is given by[67]

$$\sigma_{dip} \approx (\bar{\mu}/ea_o)^2, \tag{3.14}$$

where $\bar{\mu}$ is the transition dipole moment and a_o is the Bohr radius. For the excitation from the ground state to first excited state the transition dipole moment is $\bar{\mu} \simeq \zeta_{01}\partial\mu/\partial\zeta$, where ζ_{01} is the matrix element between ground and first excited state $\langle 0|\zeta|1\rangle = [\hbar/2m\Omega]^{1/2}$. $\Omega/\hbar$ is the frequency and m is the

reduced mass of the vibration, respectively. $\partial\mu/\partial\zeta$ is the change of the electric dipole moment with the ζ coordinate of Xe. On the other hand, the net change in conductance σ_{res} due to the resonant tunneling is given by[68]

$$\sigma_{res} \approx \frac{\delta\epsilon^2}{(\epsilon_{\bar{F}} - \epsilon_a)^2 + (\Gamma/2)^2} \cdot \frac{(\epsilon_{\bar{F}} \pm \Omega - \epsilon_a)^2 - (\Gamma/2)^2}{(\epsilon_{\bar{F}} \pm \Omega - \epsilon_a)^2 + (\Gamma/2)^2} \tag{3.15}$$

ϵ_a is the resonance level of the atom and $\epsilon_{\bar{F}}$ is the Fermi level of the substrate. $\delta\epsilon$ is defined as

$$\delta\epsilon = \epsilon_a' \hbar/(2m \cdot \Omega)^{1/2} \tag{3.16}$$

where Γ is the width of the resonance. ϵ_a' is the derivative of the resonant level of the atom with respect to the displacement associated with a vibrational mode of the adsorbed atom. The sign in front of Ω is positive when the electrons tunnel from tip to the sample-atom system, but becomes opposite for the reverse direction. The vibration of the Xe atom is excited by both of these two mechanisms where the total net change is (the fraction of the electrons tunneling inelastically) $\sigma_{in} = \sigma_{dip} + \sigma_{res}$.

The Xe atom - metal surface dipole moment has entered into the picture since the tunneling electrons are interacting with the transition dipole moment. The induced dipole moments of rare gas atoms on metal surfaces has been the subject of great interest both experimentally and theoretically. It was experimentally shown that the adsorption of a rare gas at monolayer coverages[69] on the metal surfaces can cause work-function changes up to 1 eV, $\Delta\phi \sim 1$ eV. It is known that certain adsorbed atoms give rise to the change in the work-function ϕ of the substrate by inducing dipole moment at the surface. Adsorbate donating charge (such as alkali metal atoms) or taking charge (strongly electronegative atoms) are known to affect the work function. The dipole moments leading to such changes in the work-function have been found to be unexpectedly large for the physisorbed inert gas atoms. Theoretical predictions have generally underestimated the induced dipole moments[70-72] The static polarization due to Van der Waals interaction was found to result in negligible dipole moment.[70] Lang's calculations within local-density approximation (LDA) provide sufficient evidence that dipole moment can be as large as the observed change in the

work-function. His charge density difference contourplots show polarization and charge transfer. Moreover, Wandelt and Gumhalter pointed out that the partial occupation of the Xe 6s resonance might cause an additional dipole moment in the reverse direction of the measured dipole moment μ.[55]

The atomic energy levels of the Xe-5p and Pt-5d states lie in the same energy range. Therefore, we assume that there is a charge accumulation between the Xe atom and the Pt(111) surface both from the filled Xe-5p state and from the metal state like in a covalent bond. Lang's density difference contours for the Xe atom on a jellium surface corresponding to $r_s = 2$ support this argument. We also consider the charge transfer from the metal to the Xe-6s resonance. Finally, we express the induced total dipole moment in the form

$$\mu = \mu_C + \mu_P + \mu_{CT}. \tag{3.17}$$

Here, μ_C denotes the dipole moment due to the charge accumulation between the Xe atom and metal. μ_P is the dipole moment due to polarization of Xe atom and μ_{CT} is the dipole moment induced by the image of the excess charge on the Xe-6s resonance. The polarization is considered small and μ_P is neglected. The total dipole moment μ is found from the work-function change $\Delta\phi$ caused by the Xe adsorbed on Pt by using Topping's formula[73]

$$\Delta\phi = \frac{4\pi \times 300 N_k \mu}{(1 + 9\alpha N_k^{3/2})} \tag{3.18}$$

N_k is the surface density of the adsorbed Xe atoms. Chen et al. measured[74] $\Delta\phi$ for Xe on Pt as $\sim$ 0.96 eV for $N_k \sim 6 \times 10^{14} cm^{-2}$. The polarization of the Xe atom α is taken as $4.021 \times 10^{24} cm^3$ from reference 70. Then we calculate μ as $0.65D$ for monolayer coverage of Xe on the Pt(111) surface while Gottlieb and Bruch reported the value $0.55D$ for the same surface-adsorbate system.[75] The Topping's formula also includes the depolarization interaction between induced dipole moments. The above calculation of the total dipole moment is only for the equilibrium distance between the Xe atom and the metal surface. The variation of the dipole moment with the distance of Xe from the metal surface is also needed for the dipole excitation. To obtain this variation, we investigate the

changes in the components of the total dipole moment with adatom-surface separation. Theoretical prediction of μ_C is very difficult since one has to calculate the accumulated charge and its center of the mass between Xe and the metal surface. We assume this dipole moment in the form $\mu_C \approx C.S.\zeta$. The center of the mass is probably in the mid-point between the Xe atom and the nearest Pt atom. In the present model, we assume that the accumulated charge is proportional to the overlap S, $\langle Pt - 5d_{20}|Xe5p_z\rangle$. C is a constant which is used for fitting to the total dipole moment. μ_{CT} is due to the excess charge on the Xe-6s resonance and its image. However, it is a matter of dispute whether the image of this excess charge is produced for single Xe atom. Under these circumstances, it is order to consider both cases. Namely, we calculate the contribution of the dipole excitation with (case 2) and without μ_{CT} (case 1). In the case of finite μ_{CT}, it is equal to $2d_i q_{eff}$. Here, d_i is the distance between the Xe position and the image plane. Since the induced dipole moment at the equilibrium separation is known, the constant C is found for both cases. The overlap S for equilibrium separation is equal to $\simeq 5.51 \times 10^{-2}$. The C values are 3.528×10^{-10} esu for the case 1 and 9.0165×10^{-10} esu for the case 2. In figure 3.6, the total dipole moments as functions of ζ are shown for case 1 and case 2. The variation of μ near equilibrium position of Xe ($3.33\mathring{A}$) is much faster ($\partial\mu/\partial\zeta = 0.853$ D/bohr) in case 2. (case 1 gives $\partial\mu/\partial\zeta = 0.266$ D/bohr) Lang's calculations for $r_s = 2$ substrate gives $\partial\mu/\partial\zeta \sim 0.35$ D/bohr but this substrate corresponds to the Al(111) surface for which work-function change ($\phi \sim 0.3$ eV) is smaller then that of the Pt(111) surface. It is interesting to note in the second case μ can take negative values. This means that the work-function can increase instead of decrease for certain ranges of the Xe-surface distance.

Having obtained $\mu = \mu(\zeta)$, we calculate the transition dipole moment and inelastic tunneling ratio due to dipole mechanism. These are calculated for excitations from ground state to the first excited state for different tip-sample separations and for different bias voltages since the eigenvalues are changing. Here, we present the values calculated for $s = 9.60\mathring{A}$ and $V_B = 0.100$ V. These are $\zeta_{01} = 0.168$ bohr, $\bar{\mu} \simeq 0.045$ D, and $\sigma_{dip} \simeq 3.1 \times 10^{-4}$ for case 1. Walkup et

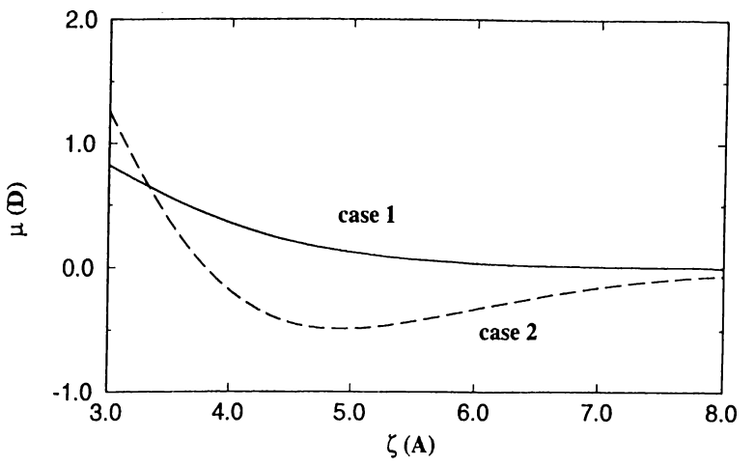

Figure 3.6: The total dipole moment μ of Xe on Pt(111) surface
The total dipole moment μ due to Xe on the Pt(111) surface as a function of ζ for case 1 (Solid line) and case 2 (Dashed line)

al. estimated the inelastic tunneling ratio due to resonant tunneling for the 6s resonance $\simeq$ 4 eV above the Fermi level with a width of $\sim$ 1 eV as $\sigma_{res} \sim 3 \times 10^{-4}$. We take this value for σ_{res}. The lifetime of the first excited state is estimated by using the elastic continuum model for several tip-sample separations and for several bias voltages. For $s = 9.60\mathring{A}$ and $V_B = 0.100$ V, the lifetime found to be $t_P \sim 19$ ps.

Excitation and relaxation of the vibration occur by the mechanism described above. Our objective is to explore the role of these mechanisms in the atom transfer. Walkup et al. argued that the atom moves on a vibrational ladder, taking steps of Δi. Their idea is based on the linear expansions for resonance and dipole mechanisms that is reminiscent of a harmonic oscillator. The rate of excitation from n-1 to n is larger than that from 0 to 1 by a factor of n. Therefore all the inelastic tunneling rates due to the dipole excitation are proportional to the rate from 0 to 1. Such processes are called linear one-step processes. The master equation for one-step processes[76] are in the form

$$\dot{P}_n = r_{n+1}P_{n+1} + g_{n-1}P_{n-1} - (r_n + g_n)P_n \tag{3.19}$$

The master equation is a gain-loss equation for the probabilities P_n for separate

states n. The r_n is the rate of fall from the state n to the state $n-1$ whereas g_n is the rate of a jump from n to $n+1$. In the linear one-step process, r_n and g_n are linear functions of n. For quantized harmonic oscillator, $r_n = \alpha n$ and $g_{n-1} = \beta n$ and the steady-state solutions are in the form

$$P_n^s = const.(\beta/\alpha)^n \tag{3.20}$$

In our case, β is equal to number of inelastic electron tunneling in one second, $\beta = (I/e).\sigma$ and α is equal to the relaxation rate $\alpha = t_P^{-1}$. Although, the atom is initially in thermal equilibrium we assume that we "heat" the sample side probabilities of the energy levels by inelastic electron tunneling after the onset of the voltage pulse. Denoting the initial occupancy of states by P_i^T and new probabilities by P_i, new probabilities can be expressed as

$$P_n = \frac{P_n^T}{F_n} + \sum_{j=0}^{n-1} P_{nj}^D \tag{3.21}$$

where F_n is a normalization factor and P_{nj}^D is the contribution from the state j to the state n. Assuming that there are L states and then defining $fc = (I/e)\sigma t_P$, F_n and P_{nj}^D are

$$F_n = 1 + fc + fc^2 + \cdots + fc^{L-n} \tag{3.22}$$

$$P_{nj}^D = \frac{P_j^T}{F_j} \cdot fc^{n-j} \tag{3.23}$$

Taking M sufficiently large, new probabilities are calculated. For the transfer rate of the Xe atom, the probabilities P_{TS}^j in equation 3.10 are replaced by the new probabilities. The transfer rates are calculated for both case 1 and case 2 for two dipole models described above. To separate the contribution of the inelastic electron tunneling, the transfer rates due to probabilities only from the excitation and relaxation (equation 3.20) are also calculated. Almost all the results of this chapter are outlined in figure 3.7.

The stars represent the rates where only excitation and relaxation are considered. The dots represent the rates for which the probabilities of the energy levels are obtained from equation 3.23 The rates without inelastic electron

tunneling (i.e rate due to the tunneling and ballistic transfer of Xe) is shown by a dashed line. Although the sample and the tip are different, the experiment of Eigler is also shown by the dots with the corresponding error bars in the same figure. One can see that the rates due to inelastic electron tunneling have a power law dependence and dominant for high voltages. At low voltages thermally assisted atom tunneling becomes more effective. The contribution of inelastic electron tunneling is strongly depended on the magnitude of the transition dipole moment. The bias voltage where the inelastic electron tunneling become dominant occurs at high bias voltages for low transition dipole moments. In case 2, the dipole excitation process start to dominate the tunneling rate at smaller voltages. Returning to the Eigler's experiment, the data except the first point shows a power law dependence on V_B. This indicates that the experiment was performed in the regimes where inelastic electron tunneling is dominant. A general conclusion, with important remarks obtained is given in the next chapter.

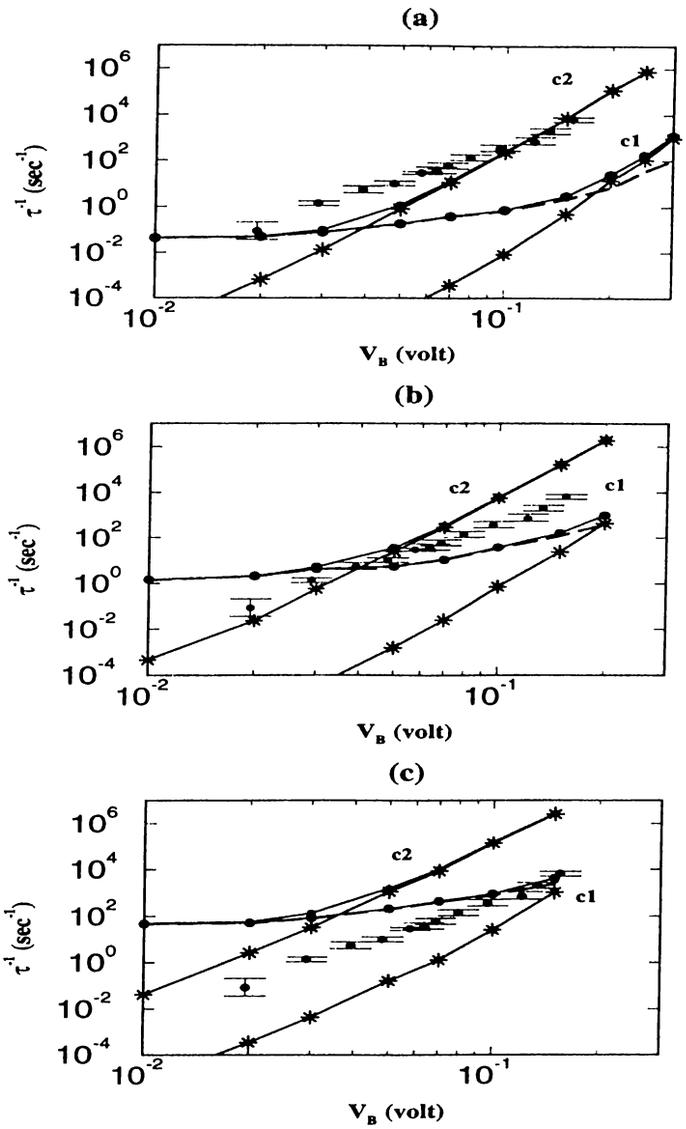

Figure 3.7: The transfer rates

The calculated transfer rates as functions of bias voltage V_B for three different tip-sample separations; (a) 9.60$\mathring{A}$, (b) 9.55$\mathring{A}$ and (c) 9.50$\mathring{A}$. The stars represent the rates where only excitation and relaxation are considered. The dots represent the rates for which the probabilities of the energy levels are obtained from equation 3.23 The rates without inelastic electron tunneling (i.e rate due to the tunneling and ballistic transfer of Xe) is shown by a dashed line. Although the sample and the tip are different, the experiment of Eigler is also shown by the dots with the corresponding error bars in the same figure.

Chapter 4

CONCLUSION

Two very important experiments performed by Eigler and his collaborators namely: i) precise repositioning of an atom on metal surfaces; ii) controlled and reversible motion of an atom realizing atomic scale switch; has been focus of this thesis work. We present theoretical investigation of the controlled lateral and perpendicular motion of atoms on metal surfaces.

The controlled lateral motion of the Xe atom on the rigid Ni(110) surface induced by the rigid W tip has been studied by using molecular statics and dynamics methods. The sharp tip was generated from the W(111) surface. The interaction between the Xe atom and the metal surface was represented by an empirical two-body Lennard-Jones potential and the potential energy surface is calculated yielding the binding site of the Xe as the hollow-site. Three different modes of motion are found in the lateral motion of Xe on the Ni(110) surface as a function of the height of the tip: 1) Pulling mode, 2) Pushing mode, 3) Carriage of Xe of the tip . Motion of Xe exhibits periodic jumps in the pulling and pushing modes. Upon allowing the tip and the sample atoms to relax, the potential barriers are modified and the translational motion is affected.

The controlled lateral motion of the Xe atom on the Pt(111) surface is studied by using a more elaborate empirical potential function including long and short-range interactions. This potential has been shown to describe a wide range of dynamical and equilibrium experimental data. The binding site of the Xe atom is

the top-site above a platinum atom and the energy barriers are lower then those on the Ni(110) surface. As compared to the case of the Ni(110) surface, Xe move more freely on the Pt(111) surface. In addition to the tip geometry and relaxation of electrodes, surface corrugation as the magnitudes, relative differences and slopes of the barriers determine the modes of motion.

We studied also the controlled and reversible transfer of the Xe atom between two flat Pt(111) surfaces. The potential energy curve has been generated from the empirical potential energy used in the lateral motion of Xe on the Pt(111) surface. The quantum states of Xe in this potential were calculated as a function of the applied voltage and the separation between two electrodes. The energy barrier for the transfer of Xe is reduced when a positive bias voltage is applied to the other electrode or when the separation is decreased. Effective charge on the Xe atom and the dipole moment were also calculated as a function of the Xe-surface separation. For the equilibrium Xe-surface separation, the effective charge on the Xe atom is $\sim -0.08|e|$ and the dipole moment is $\sim 0.65D$. The contributions of various mechanisms, such as the tunneling of Xe, dipole excitation and resonant tunneling, and electromigration, to the transfer of Xe were examined. The dependence of the rate on the separation and the bias voltage was explored. In the case of zero bias voltage, the only relevant mechanism is the thermally assisted atom tunneling. The rate is small for large two-electrode separations. On the other hand, one transfer of Xe per second may occur for separations $s \leq 9.5\mathring{A}$. The variation of the transfer rate with the separation between two Pt(111) surfaces is not smooth and shows zig-zag structure. The contribution of the thermally assisted tunneling to the transfer rate does not exhibit a power law dependence on the bias voltage; it rather shows a zig-zag structure. This can be attributed to the irregular change in the energy position of the states near the top of the barrier, which yield dominant contribution.

The transfer rate calculated only from the inelastic electron tunneling (dipole excitation and resonant tunneling) shows resemblance to the power law dependence but it dominates only for a region of the applied voltage. When both thermal assisted atom tunneling and inelastic electron tunneling are considered,

the overall behavior of the total transfer rate is not a power law. While at low bias voltages thermal assisted atom tunneling is effective, the dipole excitation and resonant tunneling becomes dominant at high bias voltages.

Bibliography

[1] G. Binnig and H. Rohrer, Helvetica Physica Acta, **55**:726, (1982)

[2] G. Binnig, C. F. Quate, and Ch. Gerber, Physical Review Letters, **49**:57, (1986)

[3] J. Tersoff and D. R. Hamann, Physical Review Letters, **50**:1998, (1983)

[4] J. Bardeen, Physical Review Letters, **6**:57 (1961)

[5] C. F. Quate, in *Highlights in Condensed Matter Physics and Future Prospects*, L.Esaki, editor, page 573, Plenum Press, New York, (1991)

[6] R. S. Becker, J. A. Golovchenko and B. S. Swartzentruber, Nature, **325**:419, (1987)

[7] M. Rigger, H. R. Hidber, R Schlögl, P. Oelhafen and H. J. Güntherodt, Applied Physics Letters, **46**:832, (1985)

[8] M. A. McCord and R. F. W. Pease, Journal of Vacuum Science and Technology, **B4**:86, (1986)

[9] I. W. Lyo and Ph. Avouris, Science, **253**:173, (1991)

[10] J. S. Foster and J. Frommer, Nature, **333**:542, (1988)

[11] J. S. Foster, J. Frommer and P. C. Arnett, Nature, **331**:324, (1988)

[12] C. W. Lin, F. R. F. Fan and A. J. Bard, Journal of Electrochemical Society, **134**:1038, (1987)

[13] L. A. Nagahara, T. Thundat and S. M. Lindsay, Reviews of Scientific Instruments, **60**:3128, (1989)

[14] U. Staufer, R. Wiesendanger, L. Eng, L. Rosenthaler, H. R. Hidber, H. J. Güntherodt and N. Garcia, Applied Physics Letters, **51**:244, (1987)

[15] J. Jahanmir, P. E. West, S. Hsieh and T. N. Rhodin, Journal of Applied Physics, **65**:2064, (1989)

[16] J. Moreland and P. Rice, Applied Physics Letters, **57**:310, (1990)

[17] R. Wiesendanger, in *Atomic and Nanometer-Scale Modificationof Materials: Fundamentals and Applications*, Ph. Avouris, editor, page 65, Kluwer Academic Publishers, Dordrecht, (1993)

[18] H. J. Mamin, P. H. Guethner and D. Rugar, Physical Review Letters, **65**:2418, (1990)

[19] E. W. Müller and T. T. Tsong, in *Field Ion Microscopy, Principles and Applications*, Elsevier, New York, (1969)

[20] D. M. Eigler and E. K. Schweizer, Nature **344**:524, (1990)

[21] D. M. Eigler, C. P. Lutz and W. E. Rudge, Nature, **352**:600, (1991)

[22] D. M. Eigler, P. S. Weiss, E. K. Schewizer, and N. D. Lang, Physical Review Letters, **66**:1189, (1991)

[23] D. M. Eigler, in *Atomic and Nanometer-Scale Modificationof Materials: Fundamentals and Applications*, Ph. Avouris, editor, page 1, Kluwer Academic Publishers, Dordrecht, (1993)

[24] S. Ciraci, E. Tekman, A. Baratoff and I. P. Batra, Physical Review B, **46**:10 411, (1991)

[25] C. Girard, D. van Labeke and J. M. Vigoureux, Physical Review B, **40**:12 133, (1989); C. Girard, *ibid.* **43**:8822, (1991)

[26] U. Hartmann, Physical Review B, **43**:2404, (1991)

[27] F. O. Goodman and N. Garcia, Physical Review B, **43**:4728, (1991)

[28] J. E. Inglesfield and E. Wikborg, J. Phys. F, **5**:1475, (1975); J. E. Inglesfield, *ibid.* **6**:687, (1976)

[29] E. Zaremba and W. Kohn, Physical Review B. **13**:2270, (1976)

[30] A. Zangwill, *Physics at Surfaces*, Cambridge University Press, Cambridge, (1988)

[31] N. D. Lang, Physical Review Letters, **46**:842. (1981)

[32] J. P. Muscat and D. M. Newns, Progress in Surface Science, **9**:1, (1978)

[33] P. W. Anderson, Physical Review, **124**:41, (1961)

[34] D. M. Newns, Physical Review, **178**:1123, (1969)

[35] S. Ciraci and A. Baratoff (unpublished); S. Ciraci, in *Atomic and Nanometer-Scale Modificationof Materials: Fundamentals and Applications*, Ph. Avouris, editor, page 111, Kluwer Academic Publishers, Dordrecht, (1993); A. Baratoff, S. Ciraci, and E. Stoll, in *13th General Conference of the Condensed Matter Division*, page 1443, (1993)

[36] U. Scheider, G. R. Castro, H. Isern, T. Janssens and K. Wandelt, Surface Science, **251/252**:551, (1991)

[37] A. Carlsson, in *Solid State Physics*, Vol. 43, H. Ehrenreich and D. Turnbull, editors, page 1, Academic Press, New York, (1990)

[38] B. E. Nieuwenhuys, O. G. van Aadenne and W. M. H. Sachter, Chemical Physics, **5**:418, (1974)

[39] M. J. Dresser, T. E. Madey and J. T. Yates, Surface Science, **42**:533, (1974)

[40] M. D. Morse, Chemical Review, **86**:1043. (1986)

[41] K. P. Huber and G. Herzberg, *Constants of Diatomic Molecules*, Van Nostrand Reinhold Com., (1979)

[42] J. R. Cerda, P. L. de Andreas, F. Flores and R. Perez, Physical Review B, **45**:8721, (1992)

[43] J. A. Barker and C. T. Rettner, Journal of Chemical Physics, **97**:5844, (1992)

[44] J. E. Müller, Physical Review Letters, **65**:3021, (1990)

[45] S. Ishi and B. Viswanathan, This Solid Films, **201**:373, (1991)

[46] M. P. Allen and D. J. Tildesley, *Computer Simulation of Liquids*, Oxford University Press, Oxford, (1987)

[47] R. Pérez, F. J. Garcia-Vidal, P. L. de Andrés and F. Flores, Surface Science, **307-309**:704, (1994)

[48] C. M. Mate, G. M. McCelland, R. Erlandsson, and S. Chiang, Physical Review Letters, **59**:1942, (1987)

[49] N. D. Lang, Physical Review B, **45**:13599, (1992)

[50] N. D. Lang, Physical Review B, **49**:2067, (1994)

[51] R. E. Walkup, D. M. Newns, and Ph. Avouris, Physical Review B, **48**:1858, (1993)

[52] G. P. Salam, M. Persson, and R. E. Palmer, Physical Review B, **49**:10655, (1994)

[53] M. Brandbyge and P. Hedegard, Physical Review Letters, **72**:2919, (1994)

[54] J. J. Sáenz and N. Garcia, Physical Review B, **47**:7537, (1993)

[55] K. Wandelt and B. Gumhalter, Surface Science, **140**:355, (1984)

[56] F. Herman and S. Skillman, *Atomic Structure Calculations*, Prentice-Hall Inc., Englewood Cliffs, New Jersey, (1963)

[57] G. Schönhense, Applied Physics A, **41**:39, (1986)

[58] B. N. J. Persson, Physical Review B, **44**:3277, (1991)

[59] S. Gao, M. Persson, and B. I. Lundqvist, Solid State Communications, **84**:271, (1992)

[60] B. N. J. Persson and R. Ryberg, Physical Review B, **32**:3586, (1985)

[61] J. A. Leiro and M. Persson, Surface Science, **207**:473, (1989)

[62] K. S. Ralls, D. C. Ralph, and R. A. Buhrman, Physical Review B, **40**:11561, (1989)

[63] A. H. Verbruggen, IBM Journal of Research and Development, **32**:93, (1988)

[64] H. B. Huntington and A. R. Grone, Journal of Physics and Chemistry of Solids, **20**:76, (1961)

[65] V. B. Fiks, Soviet Physics Solid State, **1**:12, (1959)

[66] C. Bosvieux and J. Freidel, Journal of Physics and Chemistry of Solids, **23**:123, (1962)

[67] B. N. J. Persson and J. E. Demuth, Solid State Communications, **57**:769, (1986)

[68] B. N. J. Persson and A. Baratoff, Physical Review Letters, **59**:339, (1987)

[69] J. C. P. Mignolet, Journal of Chemical Physics, **21**:1298, (1953)

[70] R. A. Kromhout and B. Linder, Chemical Physics Letters, **61**:283, (1979); R. A. Kromhout and B. Linder, Journal of Chemical Physics, **81**:2518, (1984)

[71] L. W. Bruch, Surface Science, **125**:194, (1983)

[72] D. van Labeke, J. M. Vigoureux, and Ph. Grossel, Journal of Chemical Physics, **86**:1632, (1987)

[73] J. Topping, Proceedings of the Royal Sociecty A, **114**:67, (1927)

[74] Y. C. Chen, J. E. Cunningham, and C. P. Flynn, Physical Review B, **30**:7317, (1984)

[75] J. M. Gottlieb and L. W. Bruch, Physical Review B, **44**:5759, (1991)

[76] N. G. van Kampen, *Stochastic Processes in Chemistry and Physics*, North-Holland, Elsevier Science Publishers, Amsterdam, (1992)